# Geochemistry of the Phlegraean Fields (Italy) proximal sources for major Mediterranean tephras: implications for the dispersal of Plinian & co-ignimbritic components of explosive eruptions

Emma L. Tomlinson[1*], Ilenia Arienzo[2], Lucia Civetta[2,3], Sabine Wulf[4], Victoria C. Smith[5], Mark Hardiman[6], Christine S. Lane[5], Antonio Carandente[2], Giovanni Orsi[2], Mauro Rosi[7], Wolfgang Müller[1], Matthew F. Thirlwall[1] and Martin A. Menzies[1]

[1]Department of Earth Sciences, Royal Holloway University of London, Egham, U.K.
[2] Istituto Nazionale di Geofisica e Vulcanologia, sezione di Napoli-Osservatorio Vesuviano, Napoli, Italy.
[3] Dipartimento di Scienze Fisiche, Università di Napoli Federico II, Napoli, Italy.
[4]GFZ German Research Centre for Geosciences, Section 5.2 – Climate Dynamics and Landscape Evolution, Potsdam, Germany
[5]Research Laboratory for Archaeology and the History of Art, University of Oxford, Oxford, United Kingdom
[6]Centre of Quaternary Research, Department of Geography, Royal Holloway University of London, Egham, Surrey, United Kingdom.
[7]Dipartimento di Scienze della Terra, Università di Pisa, Pisa, Italy.

## ABSTRACT

Volcanic activity at Phlegraean Fields, Italy, produced several major marker tephras over a 50 ka period. The caldera forming eruptions of the Campanian Ignimbrite (CI) and Neapolitan Yellow Tuff (NYT) are of particular importance for tephrostratigraphy in Europe. Other key eruptions from this source include the Pomici Principali (PP) and the Tufi Biancastri eruptions. We combine analyses of fresh glasses from proximal locations (i.e., juvenile clasts in proximal flow and fall deposits) with data for key tephra layers from Lago Grande di Monticchio, 120 km to the east. The micron-beam major (EMPA) and trace (LA-ICP-MS) element glass dataset allows us to: (a) Distinguish between tephra units produced from the Phlegraean Fields before and during the CI eruption (CI-series), and before and during the NYT and PP eruptions (NYT-series/PP); (b) Discriminate between the CI and the geochemically similar Pre-CI pyroclastic deposits; (c) Separate the NYT from Pre-NYT tephra units, although both major and trace elements do show significant overlap. The complex compositional overlap between Pre-NYT tephras may present a problem for tephra correlations in the 14-39 ka time window and may have resulted in incorrect proximal-distal and distal-distal correlations. The diagnostic chemical criteria detailed herein permits more accurate matching of distal tephras with their proximal equivalents and hence will improve chronostratigraphy of distal settings and give insight into tephra dispersal. We show that the dispersal of PP tephra was more limited than previously thought. The surge/fall (Lower Member) and subsequent pyroclastic density current (Upper Member) phases of the NYT eruption can be recognised

in distal settings. Both the NYT Lower and Upper Members are found in distal localities to the east of the Phlegraean Fields, however the Lower Member is found in the absence of the Upper Member in locations to the far north of Phlegraean Fields. Chemical compositions of the Plinian and ignimbrite phases of the CI eruption overlap extensively, but can be distinguished on a plot of Zr-Th.

**Key Words: Tephrostratigraphy, LA-ICP-MS, Campi Flegrei, Campanian Ignimbrite, Neapolitan Yellow Tuff, Lago Grande di Monticchio**

## 1. INTRODUCTION

Tephra layers deposited during large explosive volcanic eruptions form important isochronous marker beds in the stratigraphic record, allowing correlation between archaeological, terrestrial, marine and ice records (tephrostratigraphy). In addition, if the tephra can be correlated to a source and age of the eruption is well established, distal ash layers can be used as age markers within the stratigraphic record (tephrochronology). Furthermore, a reliable correlation between proximal and distal facies of an eruption deposit allows the eruption volume and tephra dispersal pattern to be reconstructed. Knowledge of these two parameters is important in volcanic hazards assessments and zoning of the territory in relation to the expected hazards. This is critical for active, restless and densely populated volcanoes such as the Phlegraean Fields resurgent caldera (Orsi et al., 1996, 1999a, b, 2004, 2009; Costa et al., 2009; Selva et al., 2012).

Tephra produced during the two most recent caldera forming eruptions at Phlegraean Fields (Fisher et al., 1993; Orsi et al., 1996), the Campanian Ignimbrite (CI, 39.28 ± 0.11 $^{40}Ar/^{39}Ar$ ka; De Vivo et al., 2001) and the Neapolitan Yellow Tuff (NYT, 14.9 ± 0.4 $^{40}Ar/^{39}Ar$ ka; Deino et al., 2004), provide important stratigraphic markers in European Quaternary deposits (e.g. Schmidt et al., 2002; Fedele et al., 2003; Pyle et al., 2006; Giaccio et al., 2008). The CI was the most explosive eruption of the Campanian Volcanic Zone (CVZ) and the largest known volcanic event in the Mediterranean region in the last 200 ka (Barberi et al., 1978). The CI has been correlated with distal occurrences of the Y-5 tephra in the eastern Mediterranean, central and eastern Europe and Russia (e.g. Keller et al., 1978; Thunell et al., 1979; Paterne et al., 1988; Vezzoli, 1991; Pyle et al., 2006). The CI is linked with layer TM-18 (36.77 varve ka BP) in the Lago Grande di Monticchio sediment core (Wulf et al., 2004). Some 25 ka later, activity in the Phlegraean Fields caldera produced the NYT. The NYT has been correlated with the 13.84-14.88 cal ka BP[1] C-2 tephra layer in the Tyrrhenian and Adriatic Seas (Paterne et al., 1988; Calanchi et al., 1998; Siani et al., 2004; Bourne et al.,

[1] All radiocarbon ages presented here (cal ka BP) have been calibrated using the IntCal09 or Marine09 internationally accepted calibration curves (Reimer et al., 2009) at 2$\sigma$. Year 0 is 1950 AD. Please see references for uncalibrated radiocarbon determinations.

2010) and with TM-8 (14.12 varve ka BP) in the Lago Grande di Monticchio core (Wulf et al., 2004; 2008). The smaller Pomici Principali (PP, also known as Agnano Pomici Principali) eruption dated at 11.92-12.26 cal ka BP (Smith et al., 2011) has been correlated with TM-7b (12.18 varve ka BP) in the Lago Grande di Monticchio core (Wulf et al., 2004; 2008) and has also been described in the Adriatic Sea (Paterne et al., 1988; Calanchi et al., 1998; Siani et al., 2004; Bourne et al., 2010) and several lake settings (Magne et al., 2006; Sulpizio et al., 2009; Lane et al., 2011).

Diagnostic glass chemistries for each eruption are essential in order to verify the use of PP, NYT and CI in tephrostratigraphy and tephrochronology. However, both the CI and NYT display chemical zoning in proximal deposits (Orsi et al., 1992; 1995; Civetta et al., 1997; Pappalardo et al., 2002a). In addition, a number of smaller eruptions at Phlegraean Fields also form stratigraphic markers in Quaternary deposits across the Mediterranean. These smaller eruptions were fed by trachyte and phonolite magmas with similar chemistries to the CI and NYT products. At least twelve Pre-Campanian Ignimbrite (Pre-CI) units are recognised at the Trefola Quarry (Orsi et al., 1996) spanning 59-39 ka (Pappalardo et al., 1999). Several of these eruptions produced quite thick (>10 m) proximal pyroclastic fall and density current deposits generated by high-energy explosive eruptions from vents outside the caldera (Orsi et al., 1996). At least 20 distinct tephra layers have been recognised for the same time window in the medial-distal Lago Grande di Monticchio core (Wulf et al., 2007).

Between the CI and NYT eruptions, numerous surges and minor fall deposits were generated from intra-caldera phreatomagmatic eruptions (Orsi et al., 1996). $^{40}Ar/^{39}Ar$ dated eruptions range in age from 30.3 ka (VRa) to 14.6 ka (PRe) (Pappalardo et al., 1999). These Pre-NYT units, deposited over a period of 25 ka, are known collectively as Tufi Biancastri (Rittmann, 1950). Several distal tephras are found in this time window. At least 10 Pre-NYT tephra layers are recorded in the Lago Grande di Monticchio core, with TM-9 and TM-15 being the most prominent (Wulf et al., 2004, 2007, 2008). TM-9 is linked to GM1. In distal settings GM1 comprises two tephra layers closely spaced in time and is dated at 14.2-16.2 cal ka BP (Siani et al., 2004; Aufgebauer et al., 2012). TM-15 is correlated with the 30-31 cal ka BP Y3, described in marine and terrestrial settings across the central Mediterranean (Zanchetta et al., 2008).

The aims of this study using Electron Microprobe Analysis (EMPA) and Laser Ablation Inductively Coupled Plasma Mass Spectrometry (LA-ICP-MS) of single glass shards, are: 1) to define the diagnostic major and trace element geochemistry of the PP, NYT and CI glasses and to investigate their compositional heterogeneity; 2) to use these diagnostic geochemisties to investigate the dispersal of the PP, NYT and CI tephra; and 3) to investigate the geochemistry of pyroclastic-fall and flow deposits that predate the CI and the NYT eruptions. Defining diagnostic chemistries of these Pre-CI and Pre-NYT units would not only allow them to be distinguished from the CI and NYT events, but also allows them to be used as stratigraphic markers.

## 2. GEOLOGICAL OUTLINE

The Phlegraean Fields lie in the Campanian Plain along the Tyrrhenian margin of the southern Apennines and is part of the Quaternary potassic province. The Phlegraean Fields comprises a 13 km wide nested caldera in the Gulf of Naples, formed mainly as a consequence of the eruption of the CI and NYT (Orsi et al., 1996). The caldera margins are poorly exposed and on the south lie beneath the Bay of Pozzuoli. The Phlegraean Fields has been active since at least 60 ka (Pappalardo et al., 1999) and many of the eruptions from the Phlegraean Fields had large Plinian columns (>40 km) that deposited widespread fall and flow units. Numerous eruptions have taken place since the NYT eruption during three epochs of activity (Di Vito et al., 1999) from vents located either along the faults bordering the caldera or along the extensional faults bordering the La Starza resurgent block (Orsi et al., 1996). The most recent eruption produced the Monte Nuovo tuff cone in 1538 AD (D'Oriano et al., 2005).

PP was a sub-Plinian to Plinian eruption, which dispersed pumice and ash mainly towards the east (Lirer et al., 2001). PP was dominantly phreatomagmatic and deposited alternating pumice/ash fall units and pyroclastic density currents (Smith et al., 2011), which show a progressive increase in magma discharge rate, as indicated by an increase in grain size and proportion of lithic fragments with stratigraphic height (Lirer et al., 2001). PP magmas are tephri-phonolitic to phonolitic (D'Antonio et al., 2007; Arienzo et al., 2010; Smith et al., 2011).

The NYT is the largest known trachytic phreato-Plinian eruption, extruding >40 $km^3$ dense rock equivalent (DRE) of latitic-to-trachytic magma, (Orsi et al., 1992, 1995; Wohletz et al., 1995). Deposits of the NYT are chemically zoned and were produced from three distinct magma batches, which are not related by fractional crystallisation (Orsi et al., 1995). The NYT sequence is divided into a Lower Member (LM) and an Upper Member (UM). The LM comprises a surge deposit (LM1) produced from a central vent, overlain by an alternating sequence of phreato-Plinian surge and Plinian fall deposits (LM2-LM13) all erupted from a central vent (Orsi et al., 1995; Orsi et al., 1992; Wohletz et al., 1995). The UM was erupted from multiple vents and deposited as pyroclastic density currents following column collapse (Orsi et al., 1995; Orsi et al., 1992; Wohletz et al., 1999). The poorly evolved latitic-trachitic magma dominated the end of the eruption (Orsi et al., 1992; 1995; Wohletz et al., 1995) and is not recorded in the precursor eruptions (Pabst et al., 2008).

The CI erupted at least 300 $km^3$ DRE (Fedele et al., 2003) of magma during two major phases. The first phase was Plinian and produced a column that reached a maximum height of 44 km and deposited pumice and ash predominantly to the south-east (Rosi et al., 1999). The second phase accompanied caldera collapse and was characterised by highly inflated pyroclastic density currents that flowed over the sea and crossed mountain ridges in excess of a thousand meters (Fisher et al., 1993; Ort et al., 2003). Breccias were emplaced during the course of the eruption (Fedele et al., 2008). The superposition of the variable and chemically distinct pyroclastic density currents is documented in a core drilled in the northern part of the city of Naples (Pappalardo et al., 2002a). On the basis of the reconstruction of the CI chemical stratigraphy from the drill core, we will refer to the three recognised pyroclastic density currents units as the lower, intermediate and upper flow units. The explosive phases that generated these units were fed by the most differentiated phonolitic magma, the compositionally intermediate and the least differentiated trachytic magmas, respectively (Civetta et al., 1997; Pappalardo et al., 2002a).

The CI magma chamber was compositionally zoned and is generally considered to have comprised two distinct magmas (trachytic and phonolitic), which mixed during the eruption (Fedele et al., 2008; Arienzo et al., 2009; Civetta et al., 1997; Pappalardo et al., 2002a). There is some debate as to the relationships between the trachytic and phonolitic layers. Some authors have suggested that the phonolitic cap was generated by undercooling and rapid crystallisation of the trachyte magma and later assimilation (Bohrson et al., 2006; Fowler et al., 2007; Pappalardo et al., 2008). Fedele et al., (1008) suggest that the CI magmas in the Breccia Museo formation are related by fractional crystallisation. However, the least and most evolved CI end-member magmas have different Sr- and Nd-isotope signatures suggesting that they evolved separately (Arienzo et al., 2009). The least evolved component is seen only at the end of the CI eruption (Arienzo et al., 2009; Pabst et al., 2008). This suggests late recharge of the CI chamber by trachytic magma that crystallised ca. 6 ka before eruption (Arienzo et al., 2011).

The chemical heterogeneity of the CI and NYT is believed to result mostly from recharge of the shallow reservoir by arrivals of less differentiated magmas and mixing (Orsi et al., 1995; Pabst et al., 2008; Arienzo et al., 2009). In contrast, the Pre-CI and Pre-NYT fall units each have a more restricted compositional range (Pabst et al., 2008). On the basis of geochemical and isotopic data, Pabst et al. (2008) argue that: 1) the Pre-CI eruptions represent distinct magma batches in multiple chambers, the last of which may have provided a mixing end-member for the CI, later influxed by less differentiated, less radiogenic magma; and 2) the Pre-NYT magmas evolved independently from the preceding CI magmatic system. The Pre-CI, CI and Pre-NYT, NYT are decoupled both geochemically and isotopically and show evidence of increasing crustal contamination through time since 60 ka (Di Renzo et al., 2011, D’Antonio et al., 2007; Pappalardo e al., 2002b; Pabst et al., 2008; Tonarini et al., 2004).

## 3. SAMPLES

### 3.1 Proximal Samples

The ash/tephra (<2 mm) component of Plinian and co-ignimbrite clouds can be dispersed by tropospheric and stratospheric systems and deposited in distal localities, therefore in our proximal study we have primarily sampled thick fall and flow deposits. Samples from the CI and NYT and several major Pre-CI and Pre-NYT eruptions were taken from well-studied outcrops from various locations in the Campanian Region (Fig. 1, Table 1). Numerous smaller eruptions recorded in the stratigraphy at Trefola quarry and elsewhere are described in detail in Pabst et al. (2008) and Pappalardo et al. (2002b).

The CI and NYT were both sampled at four separate localities; the Pre-CI was sampled at Trefola (TL) quarry and the Pre-NYT at Trefola and Verdolino (VR) quarries and at Ponti Rossi (PR). The PP samples come from Via Pigna. Eruptions were sampled at various levels, except for thin deposits (<2m) where only one representative sample was collected. Details of the eruptions sampled and sample localities are given in Table 1. Thirty pumice/scoria clasts were sampled from each level. Clasts were crushed and clean fragments from the interiors of each individual clast was picked and mounted in 'Stuers EpoFix' epoxy resin.

### 3.2 Lago Grande di Monticchio samples

We compare the proximal samples to distal tephra preserved within the Lago Grande di Monticchio core, discussed in detail in Narcisi, (1996) and Wulf et al. (2004, 2008). This lake provides an ideal distal archive for Campanian tephra due to its location 120 km east of the Phlegraean Fields (Fig. 1) on the dispersal axis of most eruptions (e.g. Santacroce et al., 2003). The Lago Grande di Monticchio core spans 135 ka and preserves >340 distinct tephra layers, of which >300 are thought to originate from the Campanian region (Wulf et al., 2004). The laminated sediments of the lake provide a high-precision varve age record (Wulf et al., 2008). Incremental counting error on Lago Grande di Monticchio varve ages is estimated to be 5-10 % (Brandt et al., 1999; Brauer et al., 2000; Wulf et al., 2008). We have determined the major and trace element compositions of prominent layers from this lake that were previously correlated to the PP (TM-7b), NYT (TM-8) and CI (TM-18-top and TM-18-base) and with key Campanian tephra in the Pre-NYT (TM-9, TM-15) time window. Pumice and glass shards from the Lago Grande di Monticchio tephra layers were picked and mounted in 'Stuers EpoFix' epoxy resin for analysis.

## 4. ANALYTICAL METHODS

### 4.1 Electron Micro-Probe Analysis

Major element compositions were determined using Jeol8600 electron microprobe, equipped with 4 wavelength dispersive spectrometers and SamX software, at the Research Laboratory for Archaeology and the History of Art, University of Oxford. An accelerating voltage of 15 kV, low beam current (6 nA), and defocused (10 $\mu$m) beam were used to minimize Na migration. Count times were 30 s, except for Na (10 s) and P and Cl (each 60 s). The instrument was calibrated using a suite of appropriate mineral standards. The calibration was verified using a range of secondary glass standards from the Max Planck Institute, Leipzig, Germany. Secondary glass (MPI-DING suite; Jochum et al., 2006) and mineral (Smithsonian Institute; Jarosewich, 2002) standards were analysed between and within runs. The PAP absorption correction method was used. Three replicate analyses were made on each sample and analyses with totals of <95 % were discarded. Sample totals are normalised to 100 wt% in all plots and tables. Accuracies of analyses of the MPI-DING glasses are <5 % for concentrations >0.8 wt%; concentrations <0.2 wt% are more qualitative. Analytical precision is <10 % relative standard deviation (%RSD) for analytes with concentrations >0.8 wt%. Error bars on plots show 2 s.d. of replicate analyses of StHs6/80-G and ATHO-G.

### 4.2 Laser Ablation Inductively Coupled Plasma Mass Spectrometry

LA-ICP-MS analyses of proximal tephra samples were performed using an Agilent 7500ce coupled to a Resonetics 193 nm ArF excimer laser-ablation system (RESOlution M-50 prototype) with a two-volume ablation cell (Müller et al., 2009) at the Department of Earth Sciences, Royal Holloway University of London. We used 57, 34 and 25 $\mu$m laser spots, depending on the size of the area available for analysis in individual samples. The repetition rate was 5 Hz and the count time was 40 s (200 pulses) on the sample and 40 s on the gas blank (background). Concentrations were calibrated using NIST612 with $^{29}$Si as the internal standard. Data reduction was performed manually using Microsoft Excel allowing removal of portions of the signal compromised by the occurrence of microcrysts, full details of the analytical and data reduction methods are given in Tomlinson et al. (2010). Accuracies of analyses of ATHO-G and StHs6/80-G MPI-DING glass analyses are typically <5 %. Reproducibility of ATHO-G analyses is <5 RSD% for all trace elements except for V (ATHO-G) and Gd (StHs6/80-G), which are close to LOD. Relative standard errors (%RSE) for sample tephra analyses are typically <2 %RSE for V, Rb, Y, Zr, Nb, La, Ce, Pr. Th, U; and <5% for Ti, Sr, Ba, Nd, Sm, Eu, Gd, <Dy, Er, Yb, Lu and Ta. Full errors (standard deviations and standard errors for individual sample analyses) are given in the supplementary information. For consistency with EMPA error reporting, error bars on plots show 2 s.d. of replicate analyses of StHs6/80-G and ATHO-G.

## 5. RESULTS

Representative major and trace element compositions of proximal pumice glasses are given in Tables 2 and 3 and of distal Lago Grande di Monticchio glass shards in Table 4. The full dataset is available as supplementary data. In this section we will highlight aspects of the chemistry that allow us to distinguish between the eruptive units, thus revealing the chemical features that can be used in proximal-distal correlations. Diagnostic ratios are summarised in Table 5. Eruptive units are described in order of increasing age consistent with the order of occurrence of tephra with increasing depth in sedimentary records.

**5.1 PP**

The PP glasses are phonolitic (56.58-58.71 wt% $SiO_2$) and extend into the tephri-phonolite field (Fig. 2) with increasing stratigraphic height. There is a negative relationship between $SiO_2$ and CaO, MgO, FeO and $TiO_2$; $K_2O$ (7.9-9.3 wt%) slightly increases with increasing $SiO_2$, while $Al_2O_3$ (18.5-19.5 wt%), MnO (0.1-0.2 wt%) and $Na_2O$ (3.3-3.9 wt%) remain approximately constant (Fig. 3a-f). PP glasses have a low degree of evolution (Zr/Sr = 0.27-0.36 and $Eu/Eu^*_N$ = 0.65-0.94) and are characterised by relatively low Th concentrations (20-29 ppm) with constant ratios of HFSE to Th (Nb/Th = 1.75 ± 0.15; Zr/Th = 10.5 ± 0.5; Y/Th = 1.0 ± 0.1; Ta/Th = 0.08 ± 0.01) and high V concentrations (94-132 ppm) (Fig. 4a-f).

PP glasses overlap extensively with the low $SiO_2$ component of the NYT- LM and -UM glasses (section 4.2), but have lower MgO (and to a lesser extent FeO) for a given $SiO_2$ content (Fig. 3a-f). Therefore, the PP and NYT units can be distinguished using major element compostions.

**5.2 NYT-series (NYT, Pre-NYT)**

Pre-NYT and NYT glasses show a negative relationship between $SiO_2$ and CaO, MgO, FeO and $TiO_2$; $K_2O$ and $Na_2O$ show an inflection at ~60 wt% $SiO_2$ with $Na_2O$ increasing and $K_2O$ decreasing at higher $SiO_2$; $Al_2O_3$ stays approximately constant (Fig. 3a-f). Chlorine is positively correlated with $Na_2O$. The Pre-NYT units form clusters at the most and least evolved ends of the array, while the NYT itself spans the whole compositional range. The NYT-series glasses have constant ratios of HFSE to Th: Nb/Th = 1.7 ± 0.1; Zr/Th = 10.9 ± 0.6; Ta/Th = 0.08 ± 0.01. They show low degrees of evolution (Fig. 4b): $Eu/Eu^*_N$ = 0.3-1.0, the largest being observed in the Pre-NYT unit TLo; Zr/Sr = 0.2-7 in most NYT-series units and 30-59 in TLo (Fig. 5f). The NYT-series has high V concentrations (20-170 ppm, Fig. 5e).

*5.2.1 NYT*

Glasses from analysed NYT-LM units (LM1, LM3, LM13) form two clusters separated by a distinct compositional gap (LM3 and LM13 both have >3.8 wt% CaO, <59 wt% $SiO_2$; LM1 has <2.6 wt% CaO and >61 wt% $SiO_2$). The LM1 glass is a trachyte (Fig. 2), and not strongly evolved (Sr/Zr = 0.4-1.8) with weak anomalies relating to feldspar fractionation ($Eu/Eu^*_N$ = 0.6-0.9; $Sr/Pr_N$ = 0.8-1.2). The LM3 and LM13 glasses are phono-trachytes (Fig. 2) and also only weakly evolved (Sr/Zr = 0.3-0.4) but with higher incompatible element concentrations and larger Eu and Sr anomalies ($Eu/Eu^*_N$ = 0.6-0.8; $Sr/Pr_N$ = 0.7-0.9) than LM1.

These two clusters represent magma 1 and magma 2 described by Orsi (1995). Glass shards of less differentiated composition (latite to trachyte), corresponding to magma 3 of Orsi et al. (1995), are not seen in this study.

Glasses from the units of the UM straddle the phonolite-trachyte boundary and span a wide compositional range between the two LM clusters and extend to less evolved compositions, with 56.0–62.1 wt% $SiO_2$ and 2.0–5.1 wt% CaO (Fig. 3) and Zr/Sr = 0.2-7.3.

In summary, NYT glasses are characterised by the following compositional features:

1. Straddle the phono-trachyte boundary at 56.0-62.1 wt% $SiO_2$.
2. The analysed LM units are bimodal with a trachytic component (<2.6 wt% CaO and >61 wt% $SiO_2$) and a phono-trachytic component (>3.8 wt% CaO, <59 wt% $SiO_2$).
3. The UM forms a continuum which overlaps with the two LM clusters and extends to less differentiated compositions.

*5.2.2 Pre-NYT*

The Pre-NYT units are collectively known as Tufi Biancastri (Rittmann, 1950), however they represent the products of several eruptions. Here we have analysed four Pre-NYT units, these are (youngest to oldest): PRa (16.1 ± 0.2 $^{40}Ar/^{39}Ar$ ka; Pappalardo et al., 1999), VRb, VRa (30.3 ± 0.2 $^{40}Ar/^{39}Ar$ ka; Pappalardo et al., 1999) and TLo. The PRa, VRb and TLo units have restricted compositional ranges, while the VRa forms two clusters.

Glasses from the Pre-NYT PRa are trachytic (Fig. 2) with 62.4 ± 0.5 wt% $SiO_2$, and 2.2 ± 0.3 wt% CaO. They are moderately enriched in trace elements (Sr/Zr = 1.3 ± 0.4; $Eu/Eu^*_N$ = 0.68 ± 0.07; $Sr/Pr_N$ = 0.23 ± 0.09) and overlap with the trachytic NYT, LM1 glasses.

Glasses from Pre-NYT VRb are trachytic (Fig. 2) with 62.2 ± 0.4 wt% $SiO_2$ and 2.2 ± 0.2 wt% CaO. In terms of trace elements, the VRb glasses are moderately enriched (Sr/Zr = 1.7 ± 1.2; Fig. 5) and largely overlap with the PRa glasses, but show a slightly wider compositional range extending to slightly higher HFSE concentrations and slightly larger feldspar related anomalies (Eu/Eu*N = 0.6 ± 0.1; Sr/PrN = 0.20 ± 0.14; Fig. 4). Glasses from unit VRb also overlap with the trachytic NYT-LM1.

Glasses from the Pre-NYT VRa are bimodal (Fig. 2-5). One population is trachytic (62.3 ± 0.4 wt% $SiO_2$, 2.2 ± 0.1 wt% CaO) with moderate enrichment levels and Eu and Sr anomalies (Sr/Zr = 1.4 ± 1.0; $Eu/Eu^*_N$ = 0.70 ± 0.15; $Sr/Pr_N$ = 0.25 ± 0.14). This cluster overlaps with trachytic NYT-LM1. The second population is phono-trachytic (58.0 ± 0.5 wt% $SiO_2$, 4.0 ± 0.3 wt% CaO), is weakly enriched (Sr/Zr = 0.34 ± 0.02; Fig. 5) and has small feldspar related anomalies ($Eu/Eu^*_N$ = 0.81 ± 0.04; $Sr/Pr_N$ = 0.86 ± 0.04; Fig 4). This cluster overlaps with the phono-trachytic NYT-LM (LM3 + LM13), but extends to slightly higher FeO and MgO for a given $SiO_2$ concentration, and has slightly lower Sr and Ba concentrations relative to the NYT.

Glasses from the Pre-NYT unit TLo are trachytic (Fig. 2) with 1.5 ± 0.1 wt% CaO and the highest $SiO_2$ and $Na_2O$ among the studied Pre-NYT units (63.9 ± 0.4 wt% $SiO_2$ and 6.0 ± 0.3 wt% $Na_2O$, respectively). The TLo glasses differ from those of the other NYT-series units, they are highly evolved (Sr/Zr = 30-59), have larger feldspar related anomalies ($Eu/Eu^*_N$ = 0.32 ± 0.04, $Sr/Pr_N$ = 0.011 ± 0.04) and contain higher concentrations of other incompatible elements (Fig 4, 5). The TLo can be distinguished from the NYT on the basis that it has significantly higher HFSE and Th concentrations (Fig 5a,b).

In summary:

1. It is extremely difficult to distinguish products of the Pre-NYT eruptions from the NYT using major and trace element geochemistry.
2. The trachytic component of the NYT-LM1 overlaps with the Pre-NYT units PRa, VRb and the trachytic population of VRa.
3. The phono-trachytic component of the NYT-LM (LM3 and LM13) overlaps with the phono-trachytic component of Pre-NYT unit VRa.
4. VRa is distinctive among the studied Pre-NYT eruptions as it is bimodal. It can be distinguished from the other studied Pre-NYT units on the basis of slightly higher MgO and FeO and lower Ba and Sr.
5. Glasses from the Pre-NYT units have slightly lower V concentrations than those from the NYT deposits.
6. The compositional overlap within the Pre-NYT coupled with the number of Pre-NYT units, mean that it is difficult to distinguish between the Pre-NYT eruptions.
7. TLo is clearly distinguished from the other Pre-NYT units studied herein, but indicates the occurrence of more evolved Pre-NYT magmas.

### 5.3 CI-series (CI, Pre-CI)

Pre-CI and CI glasses have a narrow range of CaO, MgO, FeO, $TiO_2$ (1.3-2.2, 0.26-0.52, 2.4-3.5 and 0.34-0.46 wt%, respectively) for a wide range of $SiO_2$ contents (55-63 wt%) (Fig. 3). Concentrations of $SiO_2$, $Al_2O_3$ and $K_2O$ are clustered within the Pre-CI units and the CI fall deposits. Within these units, $K_2O$ and $Al_2O_3$ decrease with increasing $SiO_2$; this trend continues in a stepwise manner through the studied Pre-CI units to the CI. Chlorine and $Na_2O$ are also clustered and show a positive correlation, but are slightly higher in the Pre-CI samples relative to CI. In contrast to the Pre-CI units and the CI fall, glasses from the CI lower and intermediate flows have a wider range of $SiO_2$ contents and $SiO_2$ is positively correlated with $Al_2O_3$ and $K_2O$. Geochemical variation within the CI is consistent with mixing between the evolved CI magma (erupted as both fall and the lower and intermediate flows) and a less evolved magma (Civetta et al., 1997; Arienzo et al., 2009). The CI upper flow, which was deposited at the end of the eruption, is less evolved and isotopically distinct from the rest of the CI-series (Arienzo et al., 2009).

Incompatible element concentrations define positive linear correlations within the CI-series (Fig. 5), except for those elements that are depleted during feldspar fractionation (Eu, Sr, Ba). Ratios of HFSE to Th are constant within the CI-series glasses (Nb/Th = 2.4 ± 0.3; Zr/Th = 13 ± 1; Ta/Th = 0.11 ± 0.01). Relative to the NYT-series, the CI-series has a higher Th concentration, higher HFSE contents, higher ratios of HFSE to Th, and low V concentrations (11-26 ppm). The CI-series also has larger Eu anomalies ($Eu/Eu^*_N$ = 0.2-0.5) than in the NYT series. The higher degree of evolution of the CI-series can also be seen in the ratio Zr/Sr = 5-84 (Fig. 5f).

*5.3.1 CI*

Glasses from the CI fall and from the lower and intermediate flow units straddle the trachyte-phonolite boundary and overlap extensively in major element composition (Fig. 2,3). In terms of trace elements, the fall is compositionally intermediate to evolved, with Zr/Sr = 5-31 (Fig. 5f) and shows negative anomalies in Sr ($Sr/Pr_N$ = 0.01-0.08) and Eu ($Eu/Eu^*_N$ = 0.24–0.34) consistent with feldspar fractionation (Fig. 4c). Glasses from the lower and intermediate flow units overlap widely with those from the fall and are also compositionally intermediate to evolved in composition, with Zr/Sr = 8-28. However, glasses from the lower and intermediate flows lack the most enriched compositions present in the CI fall and feldspar related anomalies are not so prominent ($Sr/Pr_N$ = 0.01-0.04; $Eu/Eu^*_N$ = 0.27–0.36). Concentrations of incompatible elements that are not affected by feldspar fractionation are typically lower in glasses from the lower and intermediate flows (Th = 41-51, Ba = 15-65; Nb = 13-117) than in the fall (Th = 41-62; Ba = 13-105; Nb = 13-136) components of the CI. The fall and flow (lower and intermediate) can be most clearly distinguished on a plot of Zr-Th (Fig. 6).

The magma feeding the CI upper flow unit is distinctive from the magma feeding the underlying fall and flows, as it is a trachyte (Fig. 2). The CI upper flow glasses have higher concentrations of CaO, MgO, $K_2O$ (2.5, 0.76 and 8.1 wt%, respectively) and V (<64 ppm), and lower $Na_2O$ (2.8-4.9 wt%) than the CI fall and lower/intermediate flows (Fig. 3, 5). They have ratios of $Na_2O/K_2O$ <0.6. The analysed glasses extend to poorly evolved compositions with Zr/Sr = 0.4 and negligible Eu and Sr anomalies ($Eu/Eu^*_N$ = 1.1; $Sr/Pr_N$ = 0.7). Ratios of HFSE to Th are higher than for the glasses from the CI fall and lower and intermediate flows and are transitional, with more evolved samples plotting close to the CI fall and lower/intermediate flow compositions and a less evolved magma composition.

In summary, the CI analysed glasses are characterised by the following features:

1. Glasses from the fall and the lower and intermediate flows straddle the phono-trachyte boundary and those from the upper flow are trachytic in composition (e.g. Arienzo et al., 2009; Civetta et al., 1997; Pappalardo et al., 2002a).
2. Glasses from the fall and the lower and intermediate flows have overlapping compositions and show a continuous range from intermediate to evolved compositions, with the flows extending to less evolved compositions. They can be separated on a plot of Zr-Th.
3. Glasses from the upper flow span a range between the CI fall and a less differentiated end-member composition and have $Na_2O/K_2O<0.6$.

*5.3.2 Pre-CI*

Pre-CI units (youngest to oldest) TLf, TLc and TLa (58 ± 3 $^{40}Ar/^{39}Ar$ ka; Pappalardo et al., 1999) all have narrow compositional ranges in both major and trace elements (Fig. 3, 5), as previously shown by Pabst et al. (2008) on the basis of whole rock compositions. Glasses from the Pre-CI units are phonolitic (Fig. 2) and are distinct from CI eruption glasses in terms of major element composition. The Pre-CI units are characterised by low $SiO_2$ and high CaO, FeO and $Al_2O_3$ concentrations relative to the CI. In addition, $Na_2O$ is higher in the Pre-CI units than in the fall and flows of the CI. The incompatible elements enrichment in the Pre-CI units decreases in the order TLa>TLc>TLf (Fig. 4d).

The TLf is the last large unit deposited prior to the eruption of the CI. Relative to the other Pre-CI units analysed, the TLf glasses have higher MgO contents and higher $K_2O$ and higher but overlapping $SiO_2$ and have lower $Na_2O$ and lower but overlapping FeO (Fig 3). In terms of trace element composition, TLf glasses are moderately evolved (Zr/Sr = 8-22) and have a smaller Eu anomaly ($Eu/Eu^*_N$ = 0.45 ± 0.06) and lower Th and HFSE element concentrations than TLa and TLc. TLf overlaps with the CI evolved component in terms of incompatible element composition, but differs in major elements.

The TLc glasses have the lowest $SiO_2$ content of the Pre-CI units analysed (58.6 ± 0.4 wt%). They are compositionally moderately evolved with moderate feldspar related anomalies (Zr/Sr = 41-58, $Eu/Eu^*_N$ = 0.31 ± 0.03). The TLc glasses overlap strongly with TLa glasses in both major and trace element composition (Fig. 3, 5), the main differences being that TLc glasses have higher $Al_2O_3$ (19.8 ± 0.3 wt%), higher but overlapping Th and lower but overlapping ratios of HFSE to Ti (Zr/Ti = 0.32 ± 0.02; Nb/Ti = 0.063 ± 0.003; Y/Ti = 0.025 ± 0.001).

The TLa glasses are intermediate between TLc and TLf for all major elements except that it has lower $Al_2O_3$ (19.6 ± 0.3 wt%). The TLa glasses show a similar degree of chemical evolution to TLc (Zr/Sr = 17-56, $Eu/Eu^*_N$ = 0.33 ± 0.06), except for lower $Al_2O_3$ (19.6 ± 0.3 wt%) and higher but overlapping ratios of HFSE to Ti (Zr/Ti = 0.34 ± 0.01; Nb/Ti = 0.066 ± 0.004; Y/Ti = 0.027 ± 0.001).

In summary:

1. The Pre-CI units TLa, TLc and TLf are clearly distinguished from the CI on the basis that they are phonolitic, while the CI is phonolite-trachyte and have lower $SiO_2$ and higher CaO, FeO and $Al_2O_3$ concentrations.
2. The Pre-CI units TLa and TLc are similar in major and trace element composition but can be distinguished from each other on the basis of $SiO_2$, $Al_2O_3$, Th and ratios of HFSE to Ti.
3. The Pre-CI unit TLf is distinct from TLa and TLc, it has lower Th, Nb, Y, Zr, and larger Eu anomalies
4. The possible presence of other Pre-CI units in distal locations means that it may be difficult to confidently distinguish between Pre-CI units.

### 5.4 Comparing the NYT- and CI-series

The CI-series (60-39 ka) and the NYT-series/PP (39-12 ka) can be distinguished using both major and trace element compositions. The most diagnostic criteria are:

1. The NYT-series have higher ratios of $CaO/SiO_2$, $MgO/SiO_2$ and $TiO_2/SiO_2$ and lower $Al_2O_3/SiO_2$ ratios and lower $Na_2O$, Cl and MnO concentrations relative to the CI-series.
2. Ratios of HFSE to Th distinguish members of the NYT-series (Nb/Th = 1.7 ± 0.1; Zr/Th = 10.9 ± 0.6; Ta/Th = 0.08 ± 0.01) and the CI-series (Nb/Th = 2.4 ± 0.3; Zr/Th = 13 ± 1; Ta/Th = 0.11 ± 0.01).
3. The CI-series (Zr/Sr = 5-84) is significantly more evolved than the NYT-series (Zr/Sr = 0.2-7).
4. Feldspar fractionation signatures are typically larger in the CI-series ($Eu/Eu^*_N$ = 0.2-0.5) than the NYT-series ($Eu/Eu^*_N$ = 0.3-1.0).
5. Vanadium concentrations are higher in the NYT-series (20-170 ppm) relative to the CI-series (11-26 ppm).

The NYT-series and CI-series trends appear to converge at the least evolved compositions (low incompatible element concentrations) on trace element plots (Fig.5a-d). Glass compositions from the CI upper flow extend between the CI fall and a composition similar to the least evolved NYT-series magma. Ratios of HFSE to Th in the CI upper flow are lower than for the rest of the CI-series (Table 5) and are also transitional between the CI- and NYT-series.

## 6. DISCUSSION

### 6.1 Proximal-distal correlation with Lago Grande di Monticchio tephra

In the following sections, we compare the proximal data to new major and trace element data for tephra in the medial-distal Lago Grande di Monticchio archive (Table 4). We use the diagnostic geochemistries defined proximally and, in some cases at Lago Grande di Monticchio, to assess distal occurrences of Phlegraean

Fields tephra in the literature. This allows an improved understanding of the dispersal of tephra from PP, NYT and CI. A summary of tephra dispersal characteristics is given in table 6.

*6.1.1 Pomici Principali (PP) & C-1/TM-7b*

Major and trace element analyses indicate that the PP can be distinguished from the NYT-series tephras on the basis of lower MgO and FeO for a given $SiO_2$ concentration (Fig 3b,c). Trace element compositions of the PP and NYT-series overlap widely (Fig. 4a).

The PP is correlated with TM-7b in Lago Grande di Monticchio (Narcisi, 1996; Wulf et al., 2004; Smith et al., 2011). Major and trace element data for TM-7b glasses is given in table 4. TM-7b glasses show a good match with PP for all trace element ratios, including HFSE/Th and elements affected by plagioclase crystallisation (Sr, Ba, Eu) supporting a proximal-distal correlation (Fig.6a). The TM-7b glass analyses span a narrower compositional range than the PP glasses sampled at Via Pigna (Fig. 3-5, 7a).

The PP has been linked to tephra C-1 in marine cores from the South Adriatic (Paterne et al., 1988; Siani et al., 2004; Calanchi et al., 2008). The tephra compositions reported by Siani et al. (2004) and Calanchi et al. (2008) overlap with the proximal datasets reported herein and in Smith et al. (2010) and with Lago Grande di Monticchio tephra TM-7b (Fig. 8a). The C-1 tephra of Paterne et al. (1988) is more evolved than the proximal samples, but lies on the PP trend with respect to MgO-$SiO_2$ (Fig. 8a) and is considered to have been sourced from the PP eruption. In contrast, reported occurrences of C-1/PP tephra in the central Adriatic (Bourne et al., 2010; Calanchi et al., 2008) do not correlate with the proximal PP reported here or by Smith et al. (2010). Bourne et al. (2010) report a cryptotephra layer from a central Adriatic core which comprises tephra from both the NYT and PP eruptions, however the reported data all lie on the higher MgO-$SiO_2$ trend of the NYT, Bourne (2012) later correlated this layer with TM-8, rather than TM-7b on the basis of further data. Calanchi et al. (2008) report a tephra in a central Adriatic core, whose geochemistry differs significantly from the proximal PP and TM-7b. The authors linked this tephra to PP on the basis that it is comparable to TM-7a, however this LGM tephra is does not have a PP chemistry (Wulf et al., 2004). The composition of TM-7a overlaps with the NYT-series in MgO-$SiO_2$. PP is not documented in any Tyrrhenian Sea cores in the study of Paterne et al. (1988). Therefore, we suggest that the PP has not yet been found in the central Adriatic and marine occurrences of the PP are currently confined to the south Adriatic.

The PP tephra has also been reported in terrestrial cores, Lake Bled (Slovenia, Lane et al., 2011), Lake Shkodra (Albania and Montenegro, Sulpizio et al., 2010) and Lake Accesa (Italy, Mangy et al., 2006). In Lake Bled, 620 km north of Phlegraean Fields, a cryptotephra correlated to PP shows a good overlap with the proximal data reported here and extends to more evolved compositions (Fig.7a), suggesting that the PP magma spans a wider compositional range than is represented proximally. The reported mean composition of the Lake Shkodra tephra, from a location 440 km east of the Phlegraean Fields, does not lie on the PP compositional trend and appears more similar to the NYT-series glasses reported herein. The age of the layer at lake Shkodra is poorly constrained (Sulpizio et al., 2010). Finally, Magny et al. (2006) report two distinct tephra layers with characteristics similar to the PP tephra in a core from Lake Accesa, Italy, but neither PP1 nor PP2 is comparable to the proximal PP glass compositions.

This re-examination of distal occurrences of the PP suggests that the areal extent of this tephra is limited. The presence of PP tephra in the south Adriatic and absence in the central Adriatic indicates that the PP was dominantly distributed to the east. However, the occurrence of cryptotephra in Lake Bled indicates some dispersal to the north. Distal settings appear to preserve more evolved compositions than are known from the proximal deposits.

*6.1.2 The Neapolitan Yellow Tuff (NYT) & C-2/TM-8*

Major and trace element analyses of proximal glasses indicate that the NYT tephra may be distinguished from the trachytic, geochemically similar Pre-NYT tephras, on the basis of the occurrence of less evolved phono-trachytic compositions, either representing the less differentiated cluster at 57.5-58.5 wt% $SiO_2$ (NYT-LM) and/or the less differentiated portion (down to 56.0 wt% $SiO_2$) of the continuous trend (NYT-UM). The Pre-NYT VRa layer is also bimodal with a phono-trachytic component, but the NYT is separated on the basis of lower CaO and FeO (Fig. 3a,c) and higher Ba and Sr. In the following section we assess previously correlated occurrences of the NYT tephra in terms of the dispersal of the LM and UM components.

The NYT has been correlated with the Lago Grande di Monticchio tephra TM-8 (Wulf et al., 2004). The TM-8 glasses (Table 4) have two modes (61.5-62 wt% $SiO_2$ and 56.0-58.4 wt% $SiO_2$). The high-$SiO_2$ TM-8 glasses show a good match to the high-$SiO_2$ cluster in the NYT-LM, while low-$SiO_2$ TM-8 glasses overlap with the low-$SiO_2$ cluster in the NYT-LM. The TM-8 glass compositions extend to less evolved, tephra-phonolitic compositions (lower $SiO_2$, $K_2O$, $Na_2O$ and higher FeO, MgO and CaO; Fig. 3) with higher Ba and Sr concentrations and lower Zr/Sr ratios (Fig. 5) consistent with the NYT-UM and there are some shards of intermediate composition (58-61 wt% $SiO_2$), which are also associated with the NYT-UM. Therefore, both phases of the NYT eruption are recorded at Lago Grande di Monticchio (Fig. 7b,c).

The NYT has been correlated to marine tephra C-2 in distal settings up to 250 km from the Phlegraean Fields in the Tyrrhenian and Adriatic Seas (Paterne et al., 1988; Bourne et al., 2010; Calanchi et al., 1998; Siani et al., 2004). C-2 is dated at 13.84-14.88 cal ka BP in Adriatic core MD90-917. In each of the Tyrrhenian and Adriatic marine cores, the C-2 layer is characterised by the presence of low-silica glasses (<57.5 wt% $SiO_2$) and by a differentiation trend from phono-trachytic, low-$SiO_2$ to phonolitic, high-$SiO_2$ compositions (Paterne et al., 1988; Bourne et al., 2010; Calanchi et al., 1998; Siani et al., 2004). This is consistent with a correlation to the NYT rather than any of the geochemically similar Pre-NYT layers. Specifically, distal occurrences of NYT tephra in the Tyrrhenian Sea to the west and south-west of Phlegraean Fields and the Adriatic Sea to the east and north-east of Phlegraean Fields may record both the NYT-LM and NYT-UM (Fig.7b). This is clear in the PRAD218 central Adriatic core (Bourne et al., 2010) because compositional data is given for individual glass shards, allowing both the NYT-UM trend and the NYT-LM low- and high $SiO_2$ clusters to be seen. The C-2 tephra data of Paterne (1988), Calanchi et al., (1998) and Siani et al., (2004) appear to be dominated by the NYT-UM, but this is not clear because only mean tephra compositions are given, masking the compositional range and possibly the actual magma comopostion.

The NYT tephra has been identified in terrestrial cores from Lake Bled (Slovenia, Lane et al., 2011) and Längsee, Austria (Schmidt et al., 2002), approximately 620 and 650 km north of Phlegraean Fields, respectively. The correlated tephra layers are bimodal, with clusters overlapping the phono-trachytic and trachytic populations in the NYT-LM (Fig.7b).

Both the bimodal NYT-LM and the continuous NYT-UM occur in distal localities. The NYT-UM is expected to form thicker tephra layers on the basis of its larger relative volume. The NYT-UM is the dominant NYT tephra in settings to the east and west of the Phlegraean Fields. However, the NYT-LM is found in the absence of the NYT-UM in locations (to date) up to 650 km north of the Phlegraean Fields.

*6.1.3 Pre-NYT*

Numerous eruptions punctuate the time period between the CI and NYT events, five are recorded at Trefola and Verdolino, and nine at Ponti Rossi (Orsi et al., 1996). We have analysed four of these Pre-NYT units, the data indicates that this phase of Phlegraean Fields activity is characterised by repeated eruption of very similar trachytic magmas. Tephra from the Pre-NYT eruptions may be widely dispersed, at least 10 Pre-NYT tephra layers are recorded in the Lago Grande di Monticchio core, with TM-9 and TM-15 being the most prominant (Wulf et al., 2004; 2007; 2008). Several important distal tephra layers correlated with Phlegraean Fields fall in the Pre-NYT/Tufi Biancastri time window, including GM1, Lagno Amendolare and Y-3. Siani et al. (2004) propose that some previously recognised occurrences of the C-2 tephra layer (NYT) may correlate with GM1, or may contain more than a single tephra, because the close chronology of these events makes them difficult to distinguish stratigraphically.

*6.1.3.1 TM-9/GM1* has previously been linked (Wulf et al., 2004) to the youngest of the Tufi Biancastri deposits, Ponti Rossi unit PRe dated at 14.6 ± 0.4 $^{40}Ar/^{39}Ar$ ka (Pappalardo et al., 1999), which was not analysed in this study.

The TM-9 is a 2 cm thick tephra layer with a varve age of 14.56 ka BP from Lago Grande di Monticchio (Wulf et al., 2004, 2008). New major and trace element data for TM-9 glasses are given in Table 4. The major (FeO/CaO) and trace (HFSE/Th: Fig. 5) element ratios of TM-9 glasses are consistent with the NYT series. Like the proximal Pre-NYT units studied here, the TM-9 glass displays a narrow range of major (1.85-1.99 wt% CaO, 62.1-63.1 wt% $SiO_2$) and trace element compositions. However, TM-9 has higher incompatible trace element concentrations (HFSE and Th) and lower V, Ba and Sr concentrations than any of the similar proximal Pre-NYT products studied here (Fig. 3, 5). When compared to whole rock data for proximal unit PRe (Pappalardo et al., 1999), TM-9 appears to be similar, and lower $SiO_2$, $Na_2O$, Rb and Nb and higher FeO, $K_2O$, V and Ba may be within error given the differing analytical techniques, however glass geochemical data is required to fully assess the TM-9 – PRe correlation suggested by Wulf et al. (2004).

TM-9 has been linked to GM1 (Wulf et al. 2004). GM1 is thought to be sourced from the Phlegraean fields, but its type locality is a layer on the slopes of Somma-Vesuvius, where it occurs stratigraphically above the Lagno Amendolare deposits (Andronico et al., 1996; Zanchetta et al., 2000). Tephra layers correlated to GM1 are described from the Adriatic Sea, where two layers (14.7 and 15.5 cal ka BP) are found below the C-2/NYT layer (Siani et al., 2004), and from Lake Prespa, Albania where two layers are also described (Aufgebauer et al., 2012). Our data from TM-9 reveals higher $Na_2O$ and lower $K_2O$ relative to published compositions of the GM1 type-site and distal GM1 tephra (Fig.7c,d), therefore we suggest that TM-9 and GM1 may not represent the same Pre-NYT event.

*6.1.3.2 Lagno Amendolare/TM-10* The type-site for Lagno Amendolare is an outcrop on the northern flank of Vesuvius, and is characterized by a mix of light and dark coloured pumice and dated at 15.2-16.5 cal ka BP (Andronico et al., 1996). A tephra that is correlated to TM-10 is described in the Adriatic Sea (Siani et al., 2004; Bourne et al., 2010) where it is dated at 16.1-16.9 cal ka BP (Siani et al., 2004). This layer was not analysed in this study and is not discussed here.

*6.1.3.3 Y-3/TM-15* has previously been linked (Wulf et al., 2004) to the Pre-NYT Tufi Biancastri unit VRa (Di Vito et al., 2008) sampled in this study and dated at 30.3 ± 0.2 $^{40}Ar/^{39}Ar$ ka (Pappalardo et al., 1999).

TM-15 is a 29 cm thick tephra layer with a varve age of 27.26 ka BP from Lago Grande di Monticchio. New major and trace element data for TM-15 glasses are given in Table 4. The major (FeO/CaO) and trace (HFSE/Th) element ratios of TM-15 glasses (Table 4) are consistent with the Pre-NYT series. TM-15 glasses have higher MgO and FeO for a given $SiO_2$ (Fig. 3), consistent with VRa and partially overlap with the trachytic component of the bimodal VRa (the lower part of the proximal sequence). However, TM-15 extends to lower $Al_2O_3$ and $Na_2O$ and to higher $K_2O$ and to higher HFSE concentrations (Fig.6d). Therefore, we cannot confirm a correlation between VRa and TM-15. Furthermore, TM-15 lacks a phono-trachytic component, but this may be an artefact of sampling from the base of the visible tephra layer.

TM-15 has been linked to the distal Y-3 tephra, first described from an Ionian Sea core (Keller 1978). The average major element data of Y-3 from the type-site (Keller et al., 1978) overlaps with the TM-15 field defined in this study (Fig.7e,f). Y-3 tephra has also been described from a number of locations in the Mediterranean basin, including the Balkans (Wagner et al., 2008; Caron et al., 2010) and in the Adriatic (Zanchetta et al., 2008; Calanchi et al., 1998; Bourne et al., 2010), Ionian (Kraml, 1997) and Tyrrhenian (Munno and Petrosino, 2004; Paterne et al., 1988) Seas. Of these studies, only the Tyrrhenian Sea data fall within the compositional field of TM-15, while the Adriatic Sea data of Bourne et al., (2010) lie on the same high-FeO and MgO trends but do not overlap with the type site Y-3 type site of Keller (1978). It is possible that further correlations are masked by averaged datasets, however some layers previously linked to Y-3 and/or TM-15 may be related to one or more of the other Pre-NYT eruptions.

*6.1.4 Campanian Ignimbrite (CI) & Y5/TM-18*

The phono-trachytic CI is clearly distinct from the trachytic Pre-CI magmas and has lower CaO and $K_2O$ and higher $Na_2O$ relative to the younger NYT-series magmas.

The CI is correlated with tephra layer TM-18 in Lago Grande di Monticchio (Narcisi, 1996; Wulf et al., 2004). The TM-18 layer comprises a 17 cm thick basal pumice fall layer overlain by a 9 cm thick layer of vitric ash, interpreted as the co-ignimbrite fall deposit generated during the flow phase of the CI eruption by Narcisi (1996) and Wulf et al. (2004). We have analysed the major and trace element composition glasses from of both the basal pumice and the vitric ash components of layer TM-18, here termed TM-18 base and TM-18 top, respectively (Table 4). Compositions of TM-18 base glasses match that of samples from the CI fall (Fig. 6, 7f), while TM-18 top glasses overlap completely with the tephra sampled from the proximal CI lower and intermediate flows (Fig. 6, 7e).

The CI is correlated with the Y-5 ash layer, which is recognised from marine cores across the Eastern Mediterranean (e.g. Cornell et al., 1983; Keller et al., 1978) and the C-13 layer in the Tyrrhenian Sea (Paterne et al., 1988, Ton-That et al., 2001). The CI is found in terrestrial sites as far as Russia, ~2500 km from the source (Pyle et al., 2006; Giaccio et al, 2008). Costa et al. (2012) have modelled the CI dispersal and show that >3.7 million $km^2$ was covered by >5 mm of ash. The Y-5 tephra is significant from both a climatic viewpoint as it occurs near the start of Heinrich event 4 (Ton-That et al., 2001) and an archaeological perspective as it occurs within the timeframe of the European Middle to Upper Palaeolithic transition (~40 ka BP, Fedele et al., 2008). Recorded occurrences of the Y-5 tephra have a bimodal size distribution in some sites up to 1500 km from the source (Cornell et al., 1983; Sparks and Huang, 1980), which may correspond to both the fall and dilute pyroclastic current phases of the CI eruption. The computational model of Costa et al. (2012) indicates that most of the tephra dispersal was associated with the dilute pyroclastic density current phase of the CI eruption.

Published bulk trace element compositions of distal CI tephra fall from the Aegean (Hardiman et al., 1999; Pyle et al., 2006) and Tyrrhenian (Paterne 1988; Ton-That et al., 2001) seas and from continental settings in Lesvos, Greece (Margari et al., 2007), Dobrogea, Romania (Veres et al., 2012), lakes Ohrid and Prespa, Macedonia (Sulpizio et al., 2010); Crvena Stijena, Montenegro (Morley and Woodward 2011) and Kostenki-Borschevo, Russia (Pyle et al., 2006) lie close to the boundary between CI fall and CI lower and intermediate flow on plots of Zr-Th. Therefore it is not possible to determine whether the fall or flow phase is dominant in these locations. However, these discriminators provide the possibility of further detailing the dispersal of the two main phases of the CI eruption, as full trace element glass datasets become available for distal occurrences of CI tephra.

The upper flow, represented by the samples from San Marco Evangelista quarry (this work and Arienzo et al., 2009), is considered to have been produced by the last and least energetic eruptive phase of low volume (~20 $km^3$) and high viscosity magma (Civetta et al., 1997). Proximally, the CI upper flow is restricted mainly to the Campanian Plain, but may have fuelled detached, dilute co-ignimbrite clouds that carried ash distally. A single TM-18 top shard from the distal Lago Grande di Monticchio corresponds to the composition of the CI upper flow. More distally, Sulpizio et al., (2010) report the occurrence of three differently evolved trachytic magmas in Lakes Ohrid and Prespa (Macedonia), one of which corresponds to the upper flow. However, the upper flow is not widely reported in distal settings. We use the ratio of $Na_2O/K_2O$ <0.6 to distinguish the CI Upper Flow in published datasets of distal CI tephra, in cases where compositional data is given for individual glass shards. CI upper flow tephra is present at Kostenki-Borschevo, Russia (Pyle et al., 2006), Dobrogea, Romania (Veres et al., 2012), Crvena Stijena, Montenegro (Morley and Woodward 2011), Lakes Ohrid and Prespa, Macedonia (Sulpizio et al., 2010, Caron et al., 2010, Wagner et al., 2008, Vogel et al., 2010), Lesvos, Greece (Margari et al., 2007) and Philippi, Greece (St.Seymour et al., 2004). In most cases, the CI upper flow only constitutes a minor proportion of the population of CI tephra shards and its presence in other localities may be masked in averaged datasets. Our analysis of published datasets suggests that the CI upper flow is widely present.

*6.1.5 Pre-Campanian Ignimbrite*

The Pre-CI units described here (TLa, TLc and TLf from Trefola) all have restricted compositional ranges and can be distinguished from the CI on the basis of major element composition.

Many of the Pre-CI tephra are likelyd to be widely dispersed across the Mediterranean because of their proximal thicknesses and eastward dispersal (Di Vito et al., 2008). West of the Apennines, TLc in the Trefola Quarry has been linked to the Santa Lucia fall deposits with an age 50.95 ± 2.98 cal ka BP on the basis of glass major and whole rock trace element data (Di Vito et al., 2008). The Santa Lucia deposits are widespread and thick in the Apennine area and are also reported in the Camaldoli della Torre core (Santa Lucia) from the southern slopes of Somma-Vesuvius (Di Renzo et al., 2007). However, the EDS glass data for Santa Lucia (Di Vito et al., 2008) differs significantly from the TLc data presented here, having higher CaO, $K_2O$ and MgO and lower $Na_2O$. The trace element composition of Santa Lucia pumices has lower levels of trace element enrichment relative to TLc.

## 6.2 Implications for tephra correlations

This study of proximal glass major and trace element geochemistries from the 60-12 ka eruptive sequence of the Phlegraean Fields highlights several issues of relevance for tephrochronology.

### *6.2.1 Exposure*

Incomplete preservation due to erosion and limited exposure in urban areas at proximal localities means that some tephra units preserved distally may not be recognised proximally. For example, we are unable to identify a proximal equivalent of the distal Lago Grande di Monticchio TM-18-4 and TM-15 tephra layers. For this reason, there is a need for high quality major and trace element glass datasets from high-resolution distal archives such as the Lago Grande di Monticchio, and from other type sites in medial-distal locations.

### *6.2.2 Stratigraphic variation*

Proximal deposits from the large CI and NYT eruptions show compositional variation with stratigraphic height, reflecting heterogeneous magma systems. The range of geochemistries is an additional feature which can be used to characterise a given eruption for the purpose of correlating tephras. For example we are able to distinguish the Plinian fall and dilute pyroclastic flow phases of the CI, and the lower and Upper Members of the NYT. For this reason, average tephra compositions should not be presented; representative analyses are more informative and whole datasets are desirable. It is critical that samples are taken vertically through distal tephra layers to ensure they are representative.

*6.2.3 Long lived magma systems*

Both the 60-39 ka (CI-series) and 39-14 ka (NYT-series) time windows are characterised by magma systems which erupted several times and produced tephra which either overlap extensively or are indistinguishable in composition. This is also observed for the more recent eruptions from the Phlegraean Fields (Smith et al., 2011). Therefore, it is important to consider other close-in-time and geochemically similar magmas from a potential source volcano when assigning proximal-distal and distal-distal tephra correlations. At the Phlegraean Fields, the proximal Pre-NYT units VRa, VRb and PRa cannot be clearly distinguished using major and trace element glass geochemistry. The same holds true for the Pre-CI TLa and TLc. In the absence of a definitive geochemical fingerprint, good stratigraphic, chronological, sedimentological control is required and additional characteristics of the deposit, such as clast shape, external surface, groundmass texture are also important (e.g. Cioni et al., 2008).

*6.2.4 Petrogenesis*

The consistency of U, Th, Nb, Ta, Zr, and Y inter-element ratios (Fig. 5) within the CI-series glasses indicates that they share a parental magma, in agreement with the findings of Arienzo et al. (2009), D'Antonio et al. (2007), Di Renzo et al. (2011) and Pabst et al. (2008). Differences between the CI-series magmas primarily reflect differing degrees of differentiation, but there is no systematic increase in the degree of differentiation with time, suggesting that the CI-series magmas do not reflect a single evolving magma chamber, but instead reflect distinct magma batches which originated from the parental magma at depth and fractionated in separate shallow reservoirs, as shown by Pabst et al. (2008). This excludes the last erupted magma, the CI upper flow, which is distinct from other magmas in the CI-series. Its composition is less differentiated than the CI fall and the lower and intermediate flows and defines a mixing trend between the CI fall and a less differentiated magma.

The NYT-series and the PP glasses have consistent HFSE/Th ratios and likely share a similar parent. The NYT-series and PP magmas form compositional clusters and do not define a single differentiation trend. However, these younger magmas have lower U, Th, Nb, Ta, Zr, and Y concentrations and lower HFSE/ Th ratios (Fig. 5) relative to the CI-series, indicating that the NYT-series/PP magmas originated from a different parental magma to the older series. These results agree with previous work suggesting isotopically and geochemically different magmas for the CI-series and the NYT-series/PP (Arienzo et al., 2009; Di Renzo et al., 2007; Di Renzo et al., 2011; Pabst et al., 2008; Pappalardo et al., 1999; Pappalardo et al., 2002a; Pappalardo et al., 2002b; D’Antonio et al., 2007; Tonarini et al., 2004). Understanding the petrogenetic processes operating at the Phlegraean Fields means that we can assign an unknown Phlegraean Fields tephra to the appropriate series, even in the absence of a proximal match, because the HFSE/Th ratio is indicative of a certain parental magma (CI-series magma and NYT-series/PP magma).

Where multiple eruptions produce identical tephra, such as the Pre-NYT, it may be possible to define compositional groups. Pabst et al. (2008) identified three distinct Pre-CI magma batches thath were erupted sequentially. Bracketing the age of the first and last occurrence of each compositional group may be useful in providing age constraints on an unknown Phlegraean Fields distal tephra. This could be achieved either by dating of proximal samples or using high-resolution distal archives, such as Lago Grande di Monticchio.

## 7. CONCLUSIONS

The 60-12 ka eruptive sequence of Phlegraean Fields offers an ideal case study to investigate proximal-distal tephra correlations because of the large number of eruptions recorded proximally and in the medial-distal Lago Grande di Monticchio core. The micron-beam major and trace element glass dataset presented here indicate that:

1. CI-series (60-39 ka) and NYT-series/PP magmas (39-12 ka) were derived from geochemically different magmas, in agreement with previous isotopic studies (Di Renzo et al. (2011), and references therein). HFSE/Th and FeO/CaO ratios are constant within each series, allowing an unknown Phlegraean Fields tephra to be assigned to the appropriate series, even if the exact proximal equivalent is not known.
2. Tephra from the caldera forming NYT eruption compositionally overlaps with tephra from the smaller Pre-NYT eruptions. The NYT may be distinguished by the presence of the bimodal trachytic and phono-trachytic LM and by the UM, which spans a compositional range between trachyte and phonotrachyte. Assessment of published data for distal occurrences of NYT tephra shows that the UM is the dominant NYT tephra in settings to the east and west of Phlegraean Fields. However, the NYT-LM is found in the absence of the NYT-UM in locations to the far north of Phlegraean Fields.
3. Magma erupted during the caldera forming CI event straddle the phono-trachyte and is distinct from the preceding, lower volume Pre-CI magmas in major and trace element composition. CI glasses from the Plinian (fall) and the lower and intermediate flow phases of the eruption overlap extensively, but can be separated using a plot of Zr-Th.
4. There is extensive overlap in major and trace element composition within Pre-NYT and within the Pre-CI, making it extremely difficult to assign proximal-distal and distal-distal correlations. This means that some such correlations may not be correct. For example, we show that the TM-15 layer from Lago Grande di Monticchio is not the distal equivalent of VRa. It may be possible to recognize the compositional group of an unknown

distal Phlegraean Fields tephra and therefore constrain its stratigraphic position and age.

In addition to insights into the behavior of the magmatic feeding system, proximal-distal tephra correlations of single eruptions are important for the assessment of volcanic hazards, for example zoning of territory in relation to various dangerous eruption phenomena. Proximal-distal tephra correlations allow more precise estimates of the volume of magma extruded during a single eruption and, therefore, the definition of the eruption magnitude and intensity. Knowledge of such parameters for past eruptions of an active volcano is fundamental to evaluation of the effects of such an eruption on the environment and on climate. This is particularly relevant for volcanoes located in densely populated areas, such as the Phlegraean Fields caldera located in the densely inhabited Neapolitan area of southern Italy. The results of this study will contribute to the ongoing improvement of current volcanic hazards assessments (Orsi et al., 2004; 2009; Costa et al., 2009; Selva et al., 2012).

*Acknowledgements: This work is funded by the NERC RESET Consortium (NE/E015905/1). This is paper number ROX/0020. The authors wish to thank Roberto Sulpizio and two anonymous reviewers for thorough and constructive feedback; Paul Albert and Chris Satow for useful discussions and Neil Holloway for sample preparation.*

## REFERENCES

Arienzo I., Civetta L., Heumann A., Wörner G., and Orsi G. (2009) Isotopic evidence for open system processes within the Campanian Ignimbrite (Campi Flegrei, Italy) magma chamber. *B. Volcanol.* **71**(3), 285-300.

Andronico, D., Calderoni, G., Cioni, R., Donahue, D.J., Marianelli, P., Santacroce, R., Sbrana, A., Sulpizio, R. (1996) An Updated Chronostratigraphic Scheme of the Last 19,000 Years of Vesuvius Magmatic and Eruptive History. EOS, Electronic Supplement to the Member Newspaper of the American Geophysical Union (AGU), November 7 1996, 671-672.

Arienzo I., Heumann A., Wörner G., Civetta L., and Orsi G. (2011) Processes and timescales of magma evolution prior to the Campanian Ignimbrite eruption (Campi Flegrei, Italy). *Earth Planet. Sci. Lett.* **306**(3-4), 217-228.

Arienzo I., Moretti R., Civetta L., Orsi G., and Papale P. (2010) The feeding system of Agnano Monte Spina eruption (Campi Flegrei, Italy): Dragging the past into present activity and future scenarios. *Chem. Geol.* **270**(1-4), 135-147.

Aufebauer, A., Panagiotopoulos, K., Wagner, B., Schaebitz, F., Viehberg, F.A., Vogel, H., Zanchetta, G., Sulpizio, R., Leng, M.J. and Damaschke, M. (in press) Climate and environmental change in the Balkans over the last 17 ka recorded in sediments from Lake Prespa (Albania/F.Y.R. of Macedonia/Greece). *Quatern. Int.*

Barberi F., Innocenti F., Lirer L., Munno R., Pescatore T., and Santacroce R. (1978) The campanian ignimbrite: a major prehistoric eruption in the Neapolitan area (Italy). *B. Volcanol.*, Vol. 41, 10-31.

Bohrson W. A., Spera F. J., Fowler S. J., Belkin H. E., De Vivo B., and Rolandi G. (2006) *Chapter 13 Petrogenesis of the Campanian Ignimbrite: implications for crystal-melt separation and open-system processes from major and trace elements and Th isotopic data*. In Developments in Volcanology, 9(C), 249-288.

Bourne A. J., Lowe J. J., Trincardi F., Asioli A., Blockley S. P. E., Wulf S., Matthews I. P., Piva A., and Vigliotti L. (2010) Distal tephra record for the last ca 105,000 years from core PRAD 1-2 in the central Adriatic Sea: implications for marine tephrostratigraphy. *Quaternary Sci. Rev.,* **29**(23-24), 3079-3094.

Bourne, A.J., (2012) The late Quaternary tephrochronology of the Adriatic Region: implications for the synchronisation of marine records. University of London, unpublished PhD Thesis

Brandt U., Nowaczyk N. R., Ramrath A., Brauer A., Mingram J., Wulf S., and Negendank J. F. W. (1999) Palaeomagnetism of Holocene and Late Pleistocene sediments from Lago di Mezzano and Lago Grande di Monticchio (Italy): initial results. *Quaternary Sci Rev* **18**, 961-976.

Brauer A., Mingram J., Frank U., Gunter C., Schettler G., Wulf S., Zolitschka B., and Negendank J. F. W. (2000) Abrupt environmental oscillations during the Early Weichselian recorded at Lago Grande di Monticchio, southern Italy. *Quatern. Int.* **73/74**, 79-90.

Calanchi N., Cattaneo A., Dinelli E., Gasparotto G., and Lucchini F. (1998) Tephra layers in Late Quaternary sediments of the central Adriatic Sea. *Mar. Geol.,* **149**(1-4), 191-209.

Calanchi, N, Dinelli, E. (2008) Tephrostratigraphy of the last 170 ka in sedimentary successions from the Adriatic Sea. *J. Volcan. Geoth. Res.*, **177** (1), 81-95.

Caron, B., Sulpizio, R., Zanchetta, G., Siani, G. and Santacroce, R. (2010) The Late Holocene to Pleistocene tephrostratigraphic record of Lake Ohrid (Albania). *C. R. Geosci.*, **342** (96), 453-466.

Cioni R., D'Oriano, C., Bertagnini A. (2008). Fingerprinting ash deposits of small scale eruptions by their physical and textural features. *J. Volcan. Geoth. Res.* **177**, 277-287

Civetta L., Orsi G., Pappalardo L., Fisher R. V., Heiken G., and Ort M. (1997) Geochemical zoning, mingling, eruptive dynamics and depositional processes - The Campanian Ignimbrite, Campi Flegrei caldera, Italy. *J. Volcan. Geoth. Res.,* **75**(3-4), 183-219.

Cornell W., S. Carey S., and Sigurdsson H. (1983) Computer simulation of transport and deposition of Campanian Y-5 ash. *J. Volcan. Geoth. Res.,* **17**, 89–109.

Costa A., Dell'Erba F., Di Vito M., Isaia R., Macedonio G., Orsi G., Pfeiffer T. (2009) Tephra fallout hazard assessment at the Campi Flegrei caldera (Italy) *B. Volcan.*, **71**, 259-273

Costa, A., Folch, A., Macedonio, G., Giaccio,, B., Isaia, R., Smith, V.C. (2012)

Quantifying volcanic ash dispersal and impact of the Campanian Ignimbrite super-eruption, *Geophys. Res. Lett.*, 39 doi:10.1029/2012GL051605.

D'Antonio M., Tonarini S., Arienzo I., Civetta L., and Di Renzo V. (2007) Components and processes in the magma genesis of the Phlegraean Volcanic District, Southern Italy. In *Cenozoic volcanism in the Mediterranean area*, Vol. 418 (ed. L. Beccaluva, G. Bianchini, and M. wilson), pp. 203-220. Geological Society of America Special Publication.

De Vivo B., Rolandi G., Gans P. B., Calvert A., Bohrson W. A., Spera F. J., and Belkin H. E. (2001) New constraints on the pyroclastic eruptive history of the Campanian volcanic Plain (Italy). *Miner. Petrol.,* **73**(1-3), 47-65.

Deino A. L., Orsi G., de Vita S., and Piochi M. (2004) The age of the Neapolitan Yellow Tuff caldera-forming eruption (Campi Flegrei caldera Italy) assessed by Ar-40/Ar-39 dating method. *J. Volcan. Geoth. Res.,* **133**(1-4), 157-170.

Di Renzo V., Arienzo I., Civetta L., D'Antonio M., Tonarini S., Di Vito M. A., and Orsi G. (2011) The magmatic feeding system of the Campi Flegrei caldera: Architecture and temporal evolution. *Chem. Geol.* **281**(3-4), 227-241.

Di Renzo V., Di Vito M. A., Arienzo I., Carandente A., Civetta L., D'Antonio M., Giordano F., Orsi G., and Tonarini S. (2007) Magmatic history of Somma-Vesuvius on the basis of new geochemical and isotopic data from a deep borehole (Camaldoli della Torre). *J. Petrol.,* **48**(4), 753-784.

Di Vito M. A., Isaia R., Orsi G., Southon J., de Vita S., D'Antonio M., Pappalardo L., and Piochi M. (1999) Volcanism and deformation since 12,000 years at the Campi Flegrei caldera (Italy). *J. Volcan. Geoth. Res.,* **91**(2-4), 221-246.

Di Vito M. A., Sulpizio R., Zanchetta G., and D'Orazio M. (2008) The late Pleistocene pyroclastic deposits of the Campanian Plain: new insights into the The late Pleistocene pyroclastic deposits of the Campanian Plain: new insights into the explosive activity of Neapolitan volcanoes. *J. Volcan. Geoth. Res.*, 177(1), 19-48.

De Vivo B., Rolandi G., Gans P.B., Calvert A., Bohrson W.A., Spera F.J. and Belkin H.E. (2001) New constraints on the pyroclastic eruptive history of the Campanian volcanic Plain (Italy). In: De Vivo B, Rolandi G (eds) Mt Somma Vesuvius and Volcanism of the Campania Plain. Spec Issue Mineral Petrol 73:47–65.

D'Oriano C., Poggianti E., Bertagnini A., Cioni R., Landi P., Polacci M., and Rosi M. (2005) Changes in eruptive style during the A.D. 1538 Monte Nuovo eruption (Phlegrean Fields, Italy): the role of syn-eruptive crystallisation. *B. Volcan.*, **67**, 601-621.

Fedele F. G., Giaccio B., Isaia R., and Orsi G. (2003) The Campanian Ignimbrite eruption, Heinrich Event 4, and Palaeolithic change in Europe: a high-resolution investigation. *AGU Geophys. Monogr.* **139**, 301-327.

Fedele F. G., Giaccio B., Isaia R., Orsi G., Carroll M., and Scaillet B. (2007) The Campanian Ignimbrite Factor: Towards a Reappraisal of the Middle to Upper Palaeolithic "Transition". In *Living Under the Shadow: The Cultural Impacts of Volcanic Eruptions* (ed. J. G. a. R.Torrence), pp. 19-41. Left Coast Press.

Fedele L., Scarpati C., Lanphere M., Melluso L., Morra V., Perrotta A., and Ricci G. (2008) The Breccia Museo formation, Campi Flegrei, southern Italy: geochronology, chemostratigraphy and relationship with the Campanian Ignimbrite eruption. *B. Volcan.,* **70**(10), 189-1219.

Fisher R. V., Orsi G., Ort M., and Heiken G. (1993) Mobility of a Large-Volume Pyroclastic Flow - Emplacement of the Campanian Ignimbrite, Italy. 177(1), 19-48 **56**(3), 205-220.

Fowler S. J., Spera F., Bohrson W., Belkin H. E., and De Vivo B. (2007) Phase equilibria constraints on the chemical and physical evolution of the campanian ignimbrite. *J. Petrol.* **48**(3), 459-493.

Giaccio, B., Isaia, R., Fedele, F. G., Di Canzio, E., Hoffecker, J., Ronchitelli, A., Sinitsyn, A., Anikovich, M., and Lisitsyn, S. N. (2008). The Campanian Ignimbrite and Codola tephra layers: two temporal/stratigraphic markers for the Early Upper Palaeloithic in southern Italy and eastern Europe, *J. Volcan. Geoth. Res.,* **177**, 208–226.

Hardiman J. C. (1999) Deep sea tephra from Nisyros Island, eastern Aegean Sea, Greece. In *Volcanoes in the Quaternary*, Vol. **161** (ed. C. R. Firth and W. J. McGuire), 69-88. Geological Society, London, Special Publications.

Jarosewich, E., 2002. Smithsonian Microbeam Standards. Journal of Research of the National Institute of Standards and Technology, 107(6): 681–685.

Jochum, K.P. et al., 2006. MPI-DING reference glasses for in situ microanalysis: New reference values for element concentrations and isotope ratios. Geochem. Geophy. Geosy., 7(2).

Keller J., Ryan W. B. F., Ninkovich D., and Altherr R. (1978) Explosive volcanic activity in the Mediterranean over the past 200,000 yr as recorded in deep-sea sediments. *Geol. Soc. Am. Bull.* **89**(4), 591-604.

Kraml M. (1997) Laser-40Ar/39Ar-Datierungen an distalen marinen Tephren des jung-quart.aren mediterranen Vulkanismus. Ph.D, Albert-Ludwigs-Universit.

Lane C. S., Andric M., Cullen V. L., and Blockley S. P. E. (2011) The occurrence of distal Icelandic and Italian tephra in the Lateglacial of Lake Bled, Slovenia. *Quaternary Sci. Rev.,* **30**(9-10), 1013-1018.

Le Bas M. J. and Streckeisen A. L. (1991) The IUGS systematics of igneous rocks. *Journal of the Geological Society* **148**(5), 825-833.

Lirer L., Petrosino P., and Alberico I. (2001) Hazard assessment at volcanic fields: the Campi Flegrei case history. *J. Volcan. Geoth. Res.*, **112**(1-4), 53-73.

Magny, M., de Beaulieu, J.-L., Drescher-Schneider, R., Vannière, B., Walter-Simonnet, A.-V., Millet, L., Bossuet, G. and Peyron, O. 2006. Climatic oscillations in central Italy during the Last Glacial-Holocene transition: the record from Lake Accesa. *J. Quaternary Sci.,* **21**, 311-320.

Mangiacapra A., Moretti R., Rutherford M., Civetta L., Orsi G., and Papale P. (2008) The deep magmatic system of the Campi Flegrei caldera (Italy). *Geophys. Res. Lett.,* **35**, L21304.

Margari V., Pyle D. M., Bryant C., and Gibbard P. L. (2007) Mediterranean tephra stratigraphy revisited: Results from a long terrestrial sequence on Lesvos Island, Greece. *J. Volcan. Geoth. Res.,* **163**(1-4), 34-54.

Morley, M.W. and Woodward, J.C. (in press) The Campanian Ignimbrite (Y5) tephra at CrvenaStijena Rockshelter, Montenegro. *Quaternary Research*.

Müller W., Shelley M., Miller P., and Broude S. (2009) Initial performance metrics of a new custom-designed ArF excimer LA-ICPMS system coupled to a two-volume laser-ablation cell. *J. Anal. Atom. Spectrom.,* **24**(2), 209-214.

Munno R. and Petrosino P. (2004) New constraints on the occurrence of the Y-3 upper Pliestocene tephra marker layer in the Tyrrhenian Sea. *Il Quaternario* **17**(1), 11-20.

Narcisi B. (1996) Tephrochronology of a late quaternary lacustrine record from the Monticchio maar (Vulture volcano, Southern Italy). *Quaternary Sci. Rev.,* **15**(2-3), 155-165.

Orsi G., Civetta L., D' Antonio M., Di Girolamo P., and Piochi M. (1995) Step-Filling and Development of a 3-Layer Magma Chamber - the Neapolitan-Yellow-Tuff Case-History. *J. Volcan. Geoth. Res.*, **67**(4), 291-312.

Orsi G., Civetta L., Del Gaudio C., de Vita S., Di Vito M. A., Isaia R., Petrazzuoli S., Ricciardi G., and Ricco C. (1999a) Short-Term Ground Deformations and Seismicity in the Nested Campi Flegrei Caldera (Italy): an example of active block resurgence in a densely populated area. *J. Volcan. Geoth. Res.*, **91**, 415-451.

Orsi G., D' Antonio M., de Vita S., and Gallo G. (1992) The Neapolitan Yellow Tuff, a Large-Magnitude Trachytic PhreatoPlinian Eruption - Eruptive Dynamics, Magma Withdrawal and Caldera Collapse. *J. Volcan. Geoth. Res.*, **53**(1-4), 275-287.

Orsi G., de Vita S., Di Vito M. A., Isaia R., Nave R., and Heiken G. (2003) Facing volcanic and related hazards in the Neapolitan area. In *Earth Sciences in the Cities: A Reader*, Vol. 56 (ed. Heiken G., Fakundiny R., and Sutter J.), pp. 121-170. Am. Geophys. Un., Sp. Publ. Series.

Orsi G., de Vita S., and Di Vito M. A. (1996) The restless, resurgent Campi Flegrei nested caldera (Italy): Constraints on its evolution and configuration. *J. Volcan. Geoth. Res.*, **74**(3-4), 179-214.

Orsi G., Di Vito M. A., and Isaia R. (2004) Volcanic hazard assessment at the restless Campi Flegrei caldera. *B. Volcanol.,* **66**(6), 514-530.

Orsi G., Petrazzuoli S., and Wohletz K. (1999b) Mechanical and thermo-fluid behaviour during unrest episode at the Campi Flegrei caldera (Italy). *J. Volcan. Geoth. Res.*, **91**, 453-470.

Orsi G., Di Vito M.A., Selva J. and Marzocchi W. (2009) Long term forcast of eruption style and size at Campi Flegrei caldera (Italy). *E Planet Sci Let* **287**, 265-276

Ort M., Orsi G., Pappalardo L., and Fisher R. (2003) Anisotropy of magnetic susceptibility studies of depositional processes in the Campanian Ignimbrite, Italy. *B. Volcanol.,* **65**(1), 55-72.

Pabst S., Worner G., Civetta L., and Tesoro R. (2008) Magma chamber evolution prior to the Campanian Ignimbrite and Neapolitan Yellow Tuff eruptions (Campi Flegrei, Italy). *B. Volcanol.,* **70**(8), 961-976.

Pappalardo L., Civetta L., D'Antonio M., Deino A., Di Vito M.A., Orsi G., Carandente A., de Vita S., Isaia R., and Piochi M. (1999) Chemical and Srisotopical evolution of the Phlegraean magmatic system before the Campanian Ignimbrite and the Neapolitan Yellow Tuff eruptions. *J. Volcan. Geoth. Res.*, **91**(2-4), 141-166.

Pappalardo L., Civetta L., de Vita S., Di Vito M. A., Orsi G., Carandente A., and Fisher R. V. (2002a) Timing of magma extraction during the Campanian Ignimbrite eruption (Campi Flegrei Caldera). *J. Volcan. Geoth. Res.*, **114**(3-4), 479-497.

Pappalardo L., Ottolini L., and Mastrolorenzo G. (2008) The Campanian Ignimbrite (southern Italy) geochemical zoning: insight on the generation of a super-eruption from catastrophic differentiation and fast withdrawal. *Contrib. Mineral. and Petr.,* **156**(1), 1-26.

Pappalardo L., Piochi M., D'Antonio M., Civetta L., and Petrini R. (2002b) Evidence for multi-stage magmatic evolution during the past 60 kyr at Campi Flegrei (Italy) deduced from Sr, Nd and Pb isotope data. *J. Petrol.,* **43**(8), 1415-1434.

Paterne M., Guichard F., and Labeyrie J. (1988) Explosive activity of the South Italian volcanoes during the past 80,000 years as determined by marine tephrochronology. *J. Volcan. Geoth. Res.*, **34**(3-4), 153-172.

Paterne M., Guichard F., and Labeyrie J. (1988) Explosive activity of the South Italian volcanoes during the past 80,000 years as determined by marine tephrochronology. *J. Volcan. Geoth. Res.,* **34**(3-4), 153-172.

Perrotta A. and Scarpati C. (2003) Volume partition between the Plinian and co-ignimbrite air fall deposits of the Campanian Ignimbrite eruption. *Miner Petrol.,* **79**, 67-78.

Polacci M., Pioli L., and Rosi M. (2003) The Plinian phase of the Campanian Ignimbrite eruption (Phlegrean Fields, Italy): evidence from density measurements and textural characterization of pumice. *B. Volcanol.,* **65**(6), 418-432.

Pyle D. M., Ricketts G. D., Margari V., van Andel T. H., Sinitsyn A. A., Praslov N. D., and Lisitsyn S. (2006) Wide dispersal and deposition of distal tephra during the Pleistocene `Campanian Ignimbrite/Y5' eruption, Italy. *Quaternary Sci. Rev.,* **25**(21-22), 2713-2728.

Reimer P. J., Baillie M. G. L., Bard E., Bayliss A., Beck J. W., Blackwell P. G., Bronk Ramsey C., Buck C. E., Burr G. S., Edwards R. L., Friedrich M., Grootes P. M., Guiderson T. P., Hajdas I., Heaton T. J., Hogg A. G., Hughen K. A., Kaiser K. F., Kromer B., McCormac F. G., Manning S. W., Richards D. A., Southon J. R., Talamo S., Turney C. S. M., van der Plicht J., and Weyhenmeyer C. E. (2009) IntCal09 and Marine09 radiocarbon age calibration curves, 0-50,000 years cal BP. *Radiocarbon* **51**(4), 1111-1150.

Rittmann A. (1950) Sintesi geologica dei Campi Flegrei. *Boll. Soc. Geol. Ital.* **69**, 117–177.

Rolandi G., Bellucci F., Heizler M. T., Belkin H. E., and De Vivo B. (2003) Tectonic controls on the genesis of ignimbrites from the Campanian Volcanic Zone, southern Italy. *Miner. Petrol.*, Vol. 79, pp. 3-31.

Rosi M., Vezzoli L., Castelmenzano A., and Grieco G. (1999) Plinian pumice fall deposit of the Campanian Ignimbrite eruption (Phlegraean Fields, Italy). *Journal of Volcanology and Geothermal Research* **91**(2-4), 179-198.

Santacroce R., Cristofolini R., La Volpe, L., Orsi G., and Rosi M. (2003) Italian Active Volcanoes. *Episodes* **26**(3), 227-234.

Schmidt R., van den Bogaard C., Merkt J., and Müller J. (2002) A new Lateglacial chronostratigraphic tephra marker for the south-eastern Alps: The Neapolitan Yellow Tuff (NYT) in Längsee (Austria) in the context of a regional biostratigraphy and palaeoclimate. *Quatern. Int.,* **88**(1), 45-56.

Selva J., Orsi G., Di Vito M.A., Marzocchi W. and Sandri L. (2012) Probability hazard map for future vent opening at the Campi Flegrei caldera, Italy. *B. Volcan.*, **74**, 497-510

Seymour, St K., Christanis, K., Bouzinos, A., Papazisimou, S., Papatheodorou, G., Moran, E. and Denes, G., 2004. Tephrostratigraphy and tephrochronology in the Philippi peat basin, Macedonia, Northern Hellas (Greece). *Quatern. Int.,* **121**, 53-65.

Siani G., Sulpizio R., Paterne M., and Sbrana A. (2004) Tephrostratigraphy study for the last 18,000 C-14 years in a deep-sea sediment sequence for the South Adriatic. *Quaternary Science Reviews* **23**(23-24), 2485-2500.

Smith V. C., Isaia R., and Pearce N. J. (2011) Tephrostratigraphy and glass compositions of post-15 kyr Campi Flegrei eruptions: implications for eruption history and chronostratigraphic markers. *Quaternary Sci. Rev.* **30**(25-26), 638–3660.

Sparks R. S. J. and T.C. H. (1980) The volcanological significance of deep-sea ash layers associated with ignimbrites. *Geol. Mag.* **117**, 425–436.

Sulpizio R. (2005). Three empirical methods for the calculation of distal volume of tephra-fall deposits. *J. Volcan. Geoth. Res.*, **145**(3-4), 315-336.

Sulpizio R., Zanchetta G., D'Orazio M., Vogel H., Wagner B. (2010) Tephrostratigraphy and tephrochronology of lakes Ohrid and Prespa, Balkans. *Biogeosciences,* **7**, 3273-3288.

Sulpizio R., van Welden A., Caron B., Zanchetta G. (2010) The Holocene tephrostratigraphic record of Lake Shkodra (Albania and Montenegro). *J. Quaternary Sci.*, **25**, 633-650.

Sun S.-S. and McDonough W. F. (1989) Chemical and isotopic systematics of oceanic basalts: implications for mantle composition and processes. In *Magmatism in Ocean Basins*, Vol. 42 (ed. A. D. Saunders, Norry, M.J.), pp. 313-345. Geological Society of London Special Publication.

Thirlwall M. F. (1991) Long-Term Reproducibility of Multicollector Sr and Nd Isotope Ratio Analysis. *Chem. Geol.* **94**(2), 85-104.

Thunell R., Federman A., Sparks S., and Williams D. (1979) The age, origin, and volcanological significance of the Y-5 ash layer in the Mediterranean. *Quaternary Research* **12**(2), 241-253.

Tomlinson E. L., Thordarson T., Muller W., Thirlwall M., and Menzies M. A. (2010) Micro analysis of tephra by LA-ICP-MS - strategies, advantages and limitations assessed using the Thorsmork ignimbrite (Southern Iceland). *Chem. Geol.* **279**(3-4), 73-89.

Tonarini S., Leeman W. P., Civetta L., D'Antonio M., Ferrara G., and Necco A. (2004) B/Nb and systematics in the Phlegrean Volcanic District (PVD). *J. Volcan. Geoth. Res.*, **113**, 123-139.

Ton-That T., Singer B., and Paterne M. (2001) 40Ar/39Ar dating of latest Pleistocene (41 ka) marine tephra in the Mediterranean Sea: implications for global climate records. *Earth Planet. Sci. Lett.,* **184**(3-4), 645-658.

Veres, D., Lane, C.S., Timar-Gabor, A., hambach, U., Constantin, D., Szakács, A., Fülling, A. and Onac, B.P. (in press). The Campanian Ignimbrite/Y5 tephra layer - A regional stratigraphic marker for Isotope Stage 3 deposits in the Lower Danube region. *Quatern. Int.*

Vezzoli L. (1991) Tephra layers in Bannock Basin (Eastern Mediterranean). *Mar. Geol.,* **100**(1-4), 21-34.

Vogel H., Zanchetta G., Sulpizio R., Wagner B., Nowaczyk N. (2010). A tephrostratigraphic record for the last glacial-interglacial cycle from Lake Ohrid, Albania and Macedonia. *J.Quaternary Sci.,* **25**, 320-338.

Wagner B., Sulpizio R., Zanchetta G., Wulf S., Wessels M., Daut G., and Nowaczyk N. (2008) The last 40 ka tephrostratigraphic record of Lake Ohrid, Albania and Macedonia: a very distal archive for ash dispersal from Italian volcanoes. *J. Volcan. Geoth. Res.*, **177**(1), 71-80.

Wohletz K., Civetta L., and Orsi G. (1999) Thermal evolution of the Phlegraean magmatic system. *J. Volcan. Geoth. Res.*, **91**(2-4), 381-414.

Wohletz K., Orsi G., and de Vita S. (1995) Eruptive Mechanisms of the Neapolitan Yellow Tuff Interpreted from Stratigraphic, Chemical, and Granulometric Data. *J. Volcan. Geoth. Res.*, **67**, 263-290.

Wulf S., Brauer A., Mingram J., Zolitschka B., and Negendank J. F. W. (2007) Distal tephras in the sediments of Monticchio maar lakes. In *Geologia del Monte Vulture* (ed. C. Principe), pp. 105-122.

Wulf S., Kraml M., Brauer A., Keller J., and Negendank J. F. W. (2004) Tephrochronology of the 100 ka lacustrine sediment record of Lago Grande di Monticchio (southern Italy). *Quatern. Int.,* **122**, 7-30.

Wulf S., Kraml M., and Keller J. (2008) Towards a detailed distal tephrostratigraphy in the Central Mediterranean: The last 20,000 yrs record of Lago Grande di Monticchio. *J. Volcan. Geoth. Res.*, **177**(1), 118-132.

Zanchetta G., Di Vito M.A., Fallick A. E., and Sulpizio R. (2000) Stable isotopes of pedogenic carbonates from the Somma-Vesuvius area, Southern Italy, over the past 18 kyr: paleoclimatic implications. *J.Quaternary Sci.,* **15**(8), 813-824.

Zanchetta G., Sulpizio R., Giaccio B., Siani G., Paterne M., Wulf S., and D'Orazio M. (2008) The Y-3 tephra: A Last Glacial stratigraphic marker for the central Mediterranean basin. *J. Volcan. Geoth. Res.*, **177**(1), 145-154.

Zollo A., Maercklin N., Vassallo M., Dello Iacono D., Virieux J., and Gasparini P. (2008) Seismic reflections reveal a massive melt layer under Campi Flegrei volcanic field. *Geophys. Res. Lett.,* **244**(35), L12306.

## CAPTIONS

## Tables

Table 1: Summary of Phlegraean Fields eruptions and samples studied. Samples used in previous studies 1 - Tortora unpublished MSc thesis; 2 - Pappalardo et al. (1999); 3 - Arienzo et al. (2009), resampled 10/2008; 4 - Polacci et al. (2003). Ages are from: PP - Smith et al. (2011), NYT- De Vivo et al. (2001), CI - Deino et al. (2004) PRa, VRb and TLa - Pappalardo et al. (1999). Mineral abbreviations: san – sanidine, plg – plagioclase, cpx – clinopyroxene, bt - biotite, mag - magnetite, ap - apatite, ol - olivine.

Table 2: Representative EMPA analyses of volcanic glass selected on basis of CaO (20$^{th}$, 40$^{th}$, 60$^{th}$, 80$^{th}$ percentile for most samples, 33$^{th}$ and 66$^{th}$ percentiles for each mode of bimodal units) and ordered by increasing CaO. Major element totals are normalised to 100 wt%, the pre-normalised total is also given. a) PP, NYT and Pre-NYT eruptions; b) CI and Pre-CI eruptions. The full dataset is given as online supplementary data.

Table 3: Representative LA-ICP-MS analyses of volcanic glass selected on basis of Sr (20$^{th}$, 40$^{th}$, 60$^{th}$, 80$^{th}$ percentile for most samples, 33$^{th}$ and 66$^{th}$ percentiles for each mode of bimodal units): a) PP, NYT and Pre-NYT eruptions; b) CI and Pre-CI eruptions. The full dataset is given as online supplementary data.

Table 4: Representative major (EMPA) and trace (LA-ICP-MS) element composition of glass shards from Lago Grande di Monticcio tephra units.

Table 5: Key concentrations and ratios for geochemical fingerprinting. *Total Alkali ($Na_2O$+$K_2O$) versus Silica ($SiO_2$) (Le Bas and Streckeisen, 1991).

Table 6: Summary of information relevant to proximal-medial-distal correlations. Ages have been calibrated using the IntCal09 or Marine09 internationally accepted calibration curves (Reimer et al., 2009) at 2$\sigma$. Year 0 is 1950 AD. Please see references for uncalibrated radiocarbon determinations. Distal tephra occurrences are those supported by this study, in the case of the CI only studies with trace element data are listed.

## Figures

Figure 1: a) regional map of study area, inset shows location of: b) Map of field localities modified after Orsi et al. (2003).

Figure 2: Total alkali-silica plot (Le Bas and Streckeisen, 1991) showing the CI-series (red/orange), NYT-series (blues) and PP (green). Also shown are distal tephra layers from the Lago Grande di Monticchio core (black). Errors are 2 s.d. calculated using replicate analyses of MPI-DING StHs6/80 glass.

Figure 3: Major element biplots showing normalised compositions of glasses from the CI-series (red/orange), NYT-series (blues) and PP (green). Also shown are distal tephra layers from the Lago Grande di Monticchio core (black). Errors are 2 s.d. calculated using replicate analyses of MPI-DING StHs6/80 glass.

Figure 4: Primitive mantle normalised trace element compositions of a) NYT and PP; and b) Pre-NYT (NYT range shown for comparison); c) CI; and d) Pre-CI (CI range shown for comparison) units. Primitive mantle values are from Sun and McDonough (1989).

Figure 5: Trace element compositions of members of the PP (green), NYT-series (blues) and CI-series (red/orange). Also shown are distal tephra layers from the Lago Grande di Monticchio core (black). Reproducibility (2 s.d.) of StHs6/80-G (S) and ATHO-G (A) analyses are shown.

Figure 6: Discriminating the fall and lower/intermediate phases of the CI using Zr-Th. Line points are 35, 495 and 65, 770.

Figure 7: Trace element compositions of Lago Grande di Monticchio tephras normalised to the average composition (grey field) and compared to representative proximal compositions ($10^{th}$, $20^{th}$, $30^{th}$, $40^{th}$, $50^{th}$, $60^{th}$, $70^{th}$, $80^{th}$, $90^{th}$ Sr percentile where >20 analyses): a) TM-7b and PP; b) TM-8 and NYT-UM; c) TM-8 and NYT-LM; d) TM15 and VRa; e) TM-18 base and CI fall; f) TM-18 top and CI flow – lower/intermediate flow.

Figure 8: Example biplots for assessing proximal distal tephra correlations: a) PP/TM-7b, $MgO$-$SiO_2$; b) NYT/TM-8 $CaO$-$SiO_2$; c) GM1/TM-9 $K_2O$-$SiO_2$; d) GM1/TM-9 $MgO$-$SiO_2$; e) VRa/TM15/Y3 $Na_2O$-$SiO_2$; f) VRa/TM15/Y3 $FeO$-$SiO_2$. Proximal samples (PP in green, NYT-series in blue) and Lago Grande di Monticchio (black) symbols are as in other plots. Distal marine locations are shown in red, lake settings in orange.

Table(s)

| | | Location | Age (ka) | Unit | Unit description | Sample name | Clast description |
|---|---|---|---|---|---|---|---|
| **Pomici Principali** | Fall | Via Pigna | 11.92-12.26 cal BP | - | Sequence of seven pumice fall layers. | PP117 A[1], PP117 B3[1], PP117 D1[1], PP117 D3[1], PP117 D5[1] | Beige to brown/grey, 5-10% phenocrysts, san, plg, cpx, bt, mag, minor ap, ol. Vesicularity 40-80% |
| **Neapolitan Yellow Tuff** | UM | Ponti Rossi | 14.9± 0.4 $^{40}Ar/^{39}Ar$ | UM | Sequence of ~4 2-4 m thick pyroclastic flows. | NYT PR UM 0301 - 0304 | Yellow and brown, <3% phenocrysts, san, plg, cpx, bt, mag, minor ap. Vesicularity 60-80%. |
| | LM | San Marco Evangelista | | LM13 | Pumice and ash fall, white to grey (Woheltz et al., 1995). | NYT 02 SME LM13 | Yellow-brown, <3% phenocrysts, san, plg, cpx, bt, mag, minor ap. Vesicularity 60-80%. |
| | | San Severino | | LM3 | Zoned pumice and ash fall, white to grey, normally graded (Woheltz et al., 1995). | NYT SS LM 3 | |
| | | Trefola | | LM1 | Complex, dominated by laminated surges. | NYT TR LM 1 | |
| **Pre-NYT (Tufi biancastri)** | PRa | Ponti Rossi | 16.1±0.2 $^{40}Ar/^{39}Ar$ | - | <0.4 m surges with intercalated fall (Orsi et al., 1996). | OCF 9602 A1[2] | light beige. <1% phenocrysts, plg, san, cpx, bt, mag, minor ap. 60-80% vesicularity. |
| | VRb | Verdolino | 28 ka $^{40}Ar/^{39}Ar$ | - | 6.0 m alternating fall and surge (Orsi et al., 1996). | OCF 945 (top), OCF 946 (base)[2] | light beige. <1% phenocrysts, plg, san, cpx, bt, mag, minor ap. 60-80% vesicularity. |
| | Vra | Verdolino | | - | 4.5 m surges overlain by 0.23 m pumice fall (Orsi et al., 1996). | OCF 9603 A2, OCF 9603 A3[2] | light beige (base) to brown (top). <1% phenocrysts, plg, san, cpx, bt, mag, minor ap. 60-80% vesicularity. |
| | Tlo | Trefola | | - | 1.4-1.7 m (remobilised) fall with basal surge (Orsi et al., 1996). | OCF 9542 (top) [2] OCF 9544 (base) [2] | light beige. <1% phenocrysts, plg, san, cpx, bt, mag, minor ap. 60-80% vesicularity. |
| **Campanian Ignimbrite** | Flow | San Marco Evangelista | 39.28 ±0.11 $^{40}Ar/^{39}Ar$ | Upper flow | 2 m thick (base not exposed), ungraded (Arienzo et al., 2009) | OF3B/08[3] | Brown-black, ca. 30% phenocrysts, san, plg, cpx, bt, mag, minor ap. Vesciularity >60%. |
| | | Mondragone | | Intermediate flow | 4 m thick, light to dark grey (1- thin laminated /massive, 2a, 2b - massive) (Civetta et al., 1997). | Mond15U3[3] | <3% phenocrysys, san, plg, cpx, bt, mag, minor ap. |
| | | | | lower flow | 3 m thick, grades from light brown, to reddish, to dark grey (2a, 2b - ignimbrite) (Civetta et al., 1997). | Mond152A2_08[3] | |
| | Fall | Acquafidia | | Fall | 0.9 m inverse graded overlain by stratified pumice | OF 16A_08 | Flow-white, vesicularity 60-90% |
| | | Voscone | | Upper fall | 0.4 m - stratified – Oscillatory, gradual decrease in clast size and increase in lithics (Rosi et al., 1999). | CIVOS 80-90 to 100-110[4] | Fall – light grey at base to pink at top, vesicularity 80-90% |
| | | | | Lower fall | 0.8 m - inverse graded (Rosi et al., 1999). | CIVOS 0-10 to 70-80[4] | |
| **Pre-CI** | Tlf | Trefola | | Flow | 4.0 m ignimbrite (Orsi et al 1996). | OCF 9550[2] | grey to dark grey, <1% phenocrysts, plg, san, cpx, bt, mag, minor ap. 60-80% vesicularity. |
| | | | | Fall | 3.9 m layered fall (Orsi et al 1996). | OCF 9601 F3[2] | |
| | Tlc | Trefola | | Flow | 2m pyroclastic flow (Orsi et al 1996). | OCF 9601 C24[2] | grey to dark grey, <1% phenocrysts, plg, san, cpx, bt, mag, minor ap. 60-90% vesicularity |
| | | | | Fall | 13.3 m of <1.7m poorly sorted fall layers and subordinate surge beds (Orsi et al., 1996). | OCF 9601 C1[2] | |
| | Tla | Trefola | 58.9± 1.8 $^{40}Ar/^{39}Ar$ | Flow | >1.1 m pyroclastic flow, with scoria (Orsi et al., 1996). | OCF 9601 A1[2] | grey to dark grey, <1% phenocrysts, plg, san, cpx, bt, mag, minor ap. 50-95% vesicularity. |
| | | | | Fall | Poorly sorted fall, base not exposed | TLa_08 | |

**Table(s)**

| Event | PP | | | | NYT-UM | | | | NYT-LM | | | | Pre-NYT VRb | | | | Pre-NYT VRa | | | | Pre-NYT PRa | | | | Pre-NYT TLo | | | |
|---|---|---|---|---|---|---|---|---|---|---|---|---|---|---|---|---|---|---|---|---|---|---|---|---|---|---|---|---|
| Percen -tile | 20 | 40 | 60 | 80 | 20 | 40 | 60 | 80 | 33 | 66 | 33 | 66 | 20 | 40 | 60 | 80 | 33 | 66 | 33 | 66 | 20 | 40 | 60 | 80 | 20 | 40 | 60 | 80 |
| sample | PP117 A-1 | PP117 A-13 | PP117 D3-2 | PP117 D5-27 | NYT PR UM 0301-3 | NYT PR UM 0301-2 | NYT PR UM 0302-2 | NYT PR UM 0304-17 | NYT TR LM1-1 | NYT TR LM1-7 | NYT 02 SME LM13-6 | NYT 02 SME LM13-1 | OCF 945-3 | OCF 946-1 | OCF 945-1 | OCF 945-9 | 9603 A3-9 | 9603 A3-8 | 9603 A2-6 | 9603 A2-10 | OCF9602 A1-19 | OCF9602 A1-9 | OCF9602 A1-25 | OCF9602 A1-13 | OCF 9544-2 | OCF 9544-5 | OCF 9542-5 | OCF 9542-8 |
| Total | 95.03 | 96.63 | 95.05 | 96.51 | 97.09 | 97.00 | 99.54 | 97.64 | 96.91 | 97.77 | 98.24 | 97.98 | 96.29 | 95.55 | 97.17 | 95.90 | 99.16 | 97.58 | 96.13 | 95.60 | 96.63 | 95.48 | 95.63 | 96.02 | 95.79 | 97.27 | 96.38 | 95.48 |
| $SiO_2$ | 58.21 | 58.26 | 57.84 | 57.83 | 61.75 | 59.72 | 58.90 | 55.76 | 61.46 | 61.79 | 58.19 | 57.61 | 62.34 | 62.21 | 62.40 | 62.14 | 58.33 | 58.09 | 62.59 | 62.21 | 62.51 | 62.64 | 62.41 | 62.43 | 64.04 | 63.68 | 63.92 | 63.75 |
| $TiO_2$ | 0.52 | 0.49 | 0.54 | 0.54 | 0.45 | 0.47 | 0.51 | 0.54 | 0.37 | 0.38 | 0.65 | 0.68 | 0.43 | 0.47 | 0.46 | 0.46 | 0.67 | 0.68 | 0.42 | 0.46 | 0.40 | 0.37 | 0.35 | 0.36 | 0.39 | 0.41 | 0.40 | 0.39 |
| $Al_2O_3$ | 18.98 | 18.88 | 18.91 | 19.04 | 18.19 | 19.01 | 18.90 | 19.91 | 18.90 | 18.55 | 18.51 | 18.73 | 18.41 | 18.30 | 18.08 | 18.49 | 18.33 | 18.30 | 18.11 | 18.14 | 18.35 | 18.22 | 18.39 | 18.53 | 18.04 | 18.05 | 17.98 | 18.22 |
| MnO | 0.14 | 0.12 | 0.19 | 0.10 | 0.15 | 0.13 | 0.22 | 0.23 | 0.12 | 0.15 | 0.19 | 0.13 | 0.10 | 0.11 | 0.20 | 0.15 | 0.14 | 0.17 | 0.15 | 0.13 | 0.10 | 0.03 | 0.13 | 0.12 | 0.18 | 0.21 | 0.24 | 0.17 |
| MgO | 1.06 | 1.01 | 1.19 | 1.27 | 0.49 | 0.71 | 1.09 | 1.55 | 0.40 | 0.44 | 1.23 | 1.33 | 0.40 | 0.43 | 0.42 | 0.33 | 1.35 | 1.52 | 0.43 | 0.43 | 0.36 | 0.40 | 0.42 | 0.37 | 0.21 | 0.21 | 0.22 | 0.22 |
| FeO | 4.38 | 4.28 | 4.59 | 4.58 | 2.80 | 3.45 | 4.04 | 5.39 | 2.65 | 2.90 | 4.87 | 4.86 | 2.42 | 2.62 | 2.52 | 2.47 | 5.13 | 5.30 | 2.81 | 2.84 | 2.66 | 2.58 | 2.78 | 2.64 | 2.30 | 2.51 | 2.31 | 2.35 |
| CaO | 3.67 | 3.78 | 3.91 | 4.12 | 2.30 | 2.75 | 3.45 | 4.67 | 2.18 | 2.15 | 4.22 | 4.30 | 2.13 | 2.24 | 2.26 | 2.31 | 3.95 | 4.04 | 2.20 | 2.23 | 2.10 | 2.19 | 2.24 | 2.33 | 1.45 | 1.48 | 1.49 | 1.52 |
| $Na_2O$ | 3.51 | 3.65 | 3.50 | 3.54 | 4.44 | 3.45 | 3.68 | 3.40 | 4.35 | 4.47 | 3.50 | 3.56 | 4.73 | 4.38 | 4.69 | 4.61 | 3.34 | 3.26 | 4.32 | 4.24 | 4.69 | 4.69 | 4.23 | 3.89 | 6.13 | 6.17 | 5.97 | 5.93 |
| $K_2O$ | 8.96 | 9.02 | 8.82 | 8.48 | 8.95 | 9.93 | 8.88 | 8.13 | 9.06 | 8.62 | 8.25 | 8.42 | 8.59 | 8.83 | 8.51 | 8.58 | 8.37 | 8.24 | 8.45 | 8.83 | 8.37 | 8.37 | 8.64 | 8.90 | 6.64 | 6.62 | 6.83 | 6.83 |
| Cl | 0.58 | 0.51 | 0.51 | 0.51 | 0.50 | 0.38 | 0.33 | 0.37 | 0.52 | 0.55 | 0.39 | 0.38 | 0.46 | 0.40 | 0.45 | 0.46 | 0.40 | 0.39 | 0.52 | 0.50 | 0.45 | 0.51 | 0.41 | 0.43 | 0.64 | 0.66 | 0.63 | 0.63 |

| Event | CI upper flow | | | | CI lower/intermediate flow | | | | CI fall | | | | Pre-CI TLf | | | | Pre-CI TLc | | | | Pre-CI TLa | | | |
|---|---|---|---|---|---|---|---|---|---|---|---|---|---|---|---|---|---|---|---|---|---|---|---|---|
| Percen -ile | 20 | 40 | 60 | 80 | 20 | 40 | 60 | 80 | 20 | 40 | 60 | 80 | 20 | 40 | 60 | 80 | 20 | 40 | 60 | 80 | 20 | 40 | 60 | 80 |
| sample | OF3B/08-30 | OF3B/08-7 | OF3B/08-20 | OF3B/08-17 | MondOF15U3-13 | Mond152 A2_08-25 | MondOF 15U3-4 | Mond152 A2_08-19 | CIVOS 100110-7 | 16A_08 -1 | CIVOS 60-70-22 | 16A_08 -2 | OCF 9550-13 | OCF 9601 F3-12 | OCF 9550-2 | OCF 9601 F3-9 | OCF 9601 C24-6 | OCF 9601 C24-2 | OCF 9601 C1-13 | OCF 9601 C24-11 | OCF 9602 A1-8 | OCF 9602 A1-4 | OCF 9602 A1-10 | Tla_08-6 |
| Total | 96.23 | 95.95 | 97.18 | 97.00 | 97.25 | 95.21 | 97.93 | 96.58 | 97.16 | 95.45 | 95.75 | 95.96 | 99.47 | 97.18 | 96.77 | 97.47 | 98.17 | 98.47 | 99.18 | 98.11 | 96.44 | 96.16 | 100.3 | 96.17 |
| $SiO_2$ | 62.93 | 62.10 | 61.63 | 61.58 | 61.78 | 61.03 | 61.50 | 61.24 | 60.83 | 61.81 | 60.89 | 61.37 | 59.05 | 59.56 | 59.33 | 59.36 | 58.43 | 58.49 | 58.46 | 58.28 | 59.11 | 58.91 | 58.75 | 59.25 |
| $TiO_2$ | 0.43 | 0.45 | 0.44 | 0.42 | 0.41 | 0.45 | 0.42 | 0.45 | 0.47 | 0.44 | 0.46 | 0.40 | 0.42 | 0.37 | 0.41 | 0.40 | 0.40 | 0.38 | 0.39 | 0.41 | 0.37 | 0.42 | 0.39 | 0.38 |
| $Al_2O_3$ | 18.29 | 18.78 | 18.65 | 18.35 | 18.71 | 18.93 | 18.95 | 18.74 | 19.35 | 19.04 | 19.50 | 18.69 | 20.00 | 19.73 | 19.85 | 19.84 | 19.64 | 19.91 | 19.81 | 19.88 | 19.70 | 19.71 | 19.64 | 19.58 |
| MnO | 0.17 | 0.21 | 0.08 | 0.09 | 0.24 | 0.15 | 0.17 | 0.23 | 0.19 | 0.20 | 0.24 | 0.25 | 0.21 | 0.23 | 0.24 | 0.24 | 0.27 | 0.23 | 0.25 | 0.29 | 0.25 | 0.29 | 0.28 | 0.30 |
| MgO | 0.38 | 0.36 | 0.76 | 0.77 | 0.32 | 0.28 | 0.35 | 0.32 | 0.32 | 0.33 | 0.34 | 0.33 | 0.35 | 0.39 | 0.39 | 0.37 | 0.31 | 0.30 | 0.29 | 0.31 | 0.32 | 0.31 | 0.31 | 0.35 |
| FeO | 2.95 | 2.74 | 3.31 | 3.48 | 2.92 | 2.72 | 2.96 | 2.93 | 2.93 | 2.90 | 2.95 | 2.90 | 3.26 | 3.27 | 3.28 | 3.30 | 3.58 | 3.57 | 3.42 | 3.59 | 3.44 | 3.43 | 3.54 | 3.47 |
| CaO | 1.39 | 1.55 | 1.77 | 2.09 | 1.60 | 1.66 | 1.70 | 1.72 | 1.71 | 1.75 | 1.78 | 1.83 | 2.01 | 2.08 | 2.10 | 2.13 | 2.01 | 2.04 | 2.06 | 2.11 | 1.88 | 1.94 | 1.98 | 2.04 |
| $Na_2O$ | 4.51 | 4.43 | 3.39 | 3.16 | 5.89 | 6.54 | 5.75 | 6.36 | 6.18 | 6.12 | 6.11 | 6.13 | 5.96 | 5.72 | 5.88 | 5.81 | 7.11 | 6.72 | 7.16 | 6.93 | 6.89 | 6.77 | 6.92 | 6.63 |
| $K_2O$ | 8.47 | 8.76 | 9.72 | 9.82 | 7.28 | 7.35 | 7.42 | 7.17 | 7.35 | 6.81 | 7.14 | 7.43 | 7.98 | 7.90 | 7.77 | 7.83 | 7.39 | 7.54 | 7.34 | 7.38 | 7.34 | 7.44 | 7.40 | 7.20 |
| Cl | 0.46 | 0.62 | 0.26 | 0.25 | 0.85 | 0.89 | 0.78 | 0.84 | 0.66 | 0.62 | 0.60 | 0.66 | 0.76 | 0.75 | 0.74 | 0.73 | 0.86 | 0.82 | 0.82 | 0.83 | 0.71 | 0.80 | 0.79 | 0.79 |

**Table(s)**

| Event | PP | | | | NYT-UM | | | | NYT-LM | | | | Pre-NYT VRb | | | | Pre-NYT VRa | | | | Pre-NYT PRa | | | | Pre-NYT TLo | | | |
|---|---|---|---|---|---|---|---|---|---|---|---|---|---|---|---|---|---|---|---|---|---|---|---|---|---|---|---|---|
| Percentile | 20 | 40 | 60 | 80 | 20 | 40 | 60 | 80 | 33 | 66 | 33 | 66 | 20 | 40 | 60 | 80 | 66 | 33 | 66 | 33 | 80 | 60 | 40 | 20 | 20 | 40 | 60 | 80 |
| sample | PP117 D1-30 | PP117 08A-20 | PP117 B3-8c | PP117 08A-2 | NYT PR UM 0301-13 | NYT PR UM 0304-14 | NYT PR UM 0302-14 | NYT PR UM 0302-5 | NYT TR LM1-2 | NYT TR LM1-4 | NYT SS LM3-8 | NYT02 SME LM13-4 | OCF 945-4 | OCF 945-8 | OCF 946-9 | OCF 946-8 | OCF 9603 A3-3 | OCF 9603 A3-10 | OCF 9603 A2-7 | OCF 9603 A2-10 | OCF 9602 A1-19a | OCF 9602 A1-12 | OCF 9602 A1-14b | OCF 9602 A1-6a | OCF 9544-10 | OCF 9542-4 | OCF 9542-6 | OCF 9542-10 |
| Ti | 2451 | 2719 | 2492 | 2773 | 2618 | 2505 | 2835 | 2745 | 2603 | 2601 | 3272 | 3386 | 2632 | 2681 | 2368 | 2505 | 3413 | 3383 | 2315 | 2291 | 2489 | 2497 | 2425 | 2313 | 2361 | 2294 | 2458 | 2484 |
| V | 100 | 110 | 97 | 110 | 55 | 86 | 91 | 93 | 56 | 58 | 119 | 135 | 53 | 49 | 51 | 56 | 113 | 113 | 38 | 37 | 56 | 54 | 54 | 49 | 23 | 24 | 27 | 24 |
| Rb | 364 | 376 | 368 | 366 | 393 | 342 | 319 | 320 | 386 | 381 | 336 | 314 | 374 | 386 | 377 | 358 | 328 | 323 | 356 | 359 | 353 | 383 | 380 | 376 | 527 | 523 | 476 | 533 |
| Sr | 819 | 844 | 858 | 872 | 244 | 527 | 901 | 1066 | 259 | 286 | 755 | 804 | 162 | 176 | 248 | 315 | 736 | 708 | 276 | 236 | 329 | 272 | 246 | 236 | 16 | 19 | 21 | 22 |
| Y | 24 | 22 | 26 | 24 | 33 | 20 | 23 | 22 | 35 | 33 | 28 | 25 | 34 | 36 | 27 | 31 | 24 | 25 | 29 | 29 | 30 | 32 | 33 | 30 | 55 | 47 | 52 | 50 |
| Zr | 257 | 232 | 265 | 239 | 368.4 | 222 | 226 | 216 | 396 | 374 | 299 | 260 | 367 | 395 | 299 | 338 | 262 | 260 | 325 | 329 | 332 | 341 | 351 | 328 | 840 | 701 | 766 | 719 |
| Nb | 42 | 42 | 44 | 42 | 59.1 | 40 | 36 | 34 | 62 | 61 | 48 | 43 | 61 | 62 | 55 | 54 | 41 | 39 | 49 | 50 | 53 | 55 | 56 | 54 | 119 | 111 | 113 | 109 |
| Ba | 1680 | 1780 | 1776 | 1802 | 87.7 | 923 | 1382 | 1656 | 93 | 144 | 1321 | 1454 | 39 | 43 | 100 | 160 | 1267 | 1259 | 108 | 74 | 222 | 140 | 103 | 112 | 4 | 5 | 5 | 5 |
| La | 62 | 59 | 64 | 60 | 82.7 | 56 | 57 | 56 | 86 | 83 | 72 | 65 | 79 | 87 | 67 | 76 | 48 | 51 | 66 | 66 | 74 | 81 | 84 | 72 | 148 | 126 | 130 | 131 |
| Ce | 120 | 113 | 121 | 117 | 161 | 106 | 111 | 108 | 166 | 159 | 143 | 128 | 152 | 168 | 128 | 145 | 95 | 101 | 125 | 126 | 142 | 149 | 163 | 142 | 267 | 240 | 247 | 239 |
| Pr | 13 | 12 | 13 | 12 | 17 | 11 | 12 | 12 | 17 | 16 | 15 | 13 | 17 | 17 | 13 | 15 | 10 | 11 | 13 | 13 | 14 | 17 | 17 | 15 | 26 | 23 | 24 | 23 |
| Nd | 46 | 45 | 48 | 44 | 61.3 | 40 | 44 | 43 | 62 | 59 | 54 | 51 | 56 | 61 | 48 | 55 | 39 | 41 | 47 | 49 | 52 | 58 | 59 | 54 | 85 | 77 | 76 | 79 |
| Sm | 8.4 | <LOD | 8.4 | 9.6 | 9.5 | <LOD | 7.9 | 7.5 | 11.4 | 11.2 | 10.1 | 9.3 | <LOD | 10.8 | <LOD | 8.8 | <LOD | 8.2 | 9.3 | 7.9 | 9.1 | 10.4 | 11.4 | 9.3 | 13.7 | 12.8 | 12.2 | 11.6 |
| Eu | 2.0 | 2.1 | 2.0 | 2.0 | 2.0 | <LOD | 2.2 | 2.2 | 2.1 | 1.9 | 2.2 | 2.1 | <LOD | 2.1 | <LOD | 2.0 | <LOD | 1.9 | 1.9 | 1.8 | 1.9 | 2.1 | 2.1 | 1.8 | 1.2 | 1.1 | 1.2 | 1.1 |
| Gd | 6.2 | <LOD | 6.7 | <LOD | 7.2 | 6.8 | 5.3 | 5.7 | 7.9 | <LOD | 7.3 | 6.6 | 8.5 | 7.6 | <LOD | 7.6 | <LOD | 5.9 | 6.5 | 6.3 | 6.9 | 7.5 | 8.0 | 8.0 | 9.9 | 9.1 | 10.5 | 9.3 |
| Dy | 4.5 | 4.4 | 4.9 | 4.6 | 6.1 | 3.7 | 4.1 | 4.4 | 6.7 | 6.1 | 5.9 | 5.1 | 6.3 | 6.6 | <LOD | 5.7 | <LOD | 4.7 | 5.2 | 5.2 | 5.7 | 6.4 | 6.6 | 5.3 | 9.0 | 8.2 | 8.5 | 7.9 |
| Er | 2.2 | <LOD | 2.8 | 2.1 | 3.2 | <LOD | 2.1 | 2.1 | 3.4 | 3.3 | 2.9 | 2.5 | 3.0 | 3.4 | <LOD | 3.0 | <LOD | 2.5 | 2.8 | 2.9 | 3.0 | 3.3 | 3.4 | 3.2 | 5.4 | 4.8 | 5.2 | 4.6 |
| Yb | 2.3 | <LOD | 2.5 | <LOD | 3.1 | 2.3 | 2.0 | 2.0 | 3.2 | 3.2 | 2.9 | 2.4 | <LOD | 3.3 | <LOD | 3.1 | <LOD | 2.5 | 2.8 | 2.9 | 3.1 | 3.2 | 3.3 | 2.7 | 6.2 | 5.4 | 5.5 | 5.0 |
| Lu | 0.4 | <LOD | 0.4 | <LOD | 0.4 | <LOD | 0.3 | 0.3 | 0.5 | 0.5 | 0.4 | 0.4 | <LOD | 0.5 | <LOD | 0.4 | <LOD | 0.3 | <LOD | 0.4 | 0.4 | 0.4 | 0.4 | 0.4 | 0.9 | 0.8 | 0.7 | 0.8 |
| Ta | 2.1 | 1.8 | 2.2 | 1.7 | 2.9 | 1.8 | 1.8 | 1.6 | 3.0 | 2.9 | 2.4 | 2.0 | 2.4 | 3.0 | 2.4 | 2.8 | <LOD | 2.0 | 2.2 | 2.5 | 2.6 | 2.6 | 2.9 | 2.6 | 5.1 | 4.7 | 5.3 | 4.4 |
| Th | 24 | 20 | 26 | 22 | 35 | 20 | 21 | 20 | 37 | 35 | 29 | 25 | 30 | 36 | 25 | 32 | 21 | 22 | 25 | 27 | 31 | 32 | 33 | 31 | 79 | 68 | 70 | 63 |
| U | 8 | 7 | 9 | 8 | 11 | 8 | 7 | 7 | 12 | 11 | 9 | 8 | 9 | 12 | 9 | 10 | 7 | 8 | 8 | 9 | 10 | 10 | 10 | 10 | 26 | 23 | 24 | 23 |

Continues next page

| Event | CI upper flow | | | | CI lower/intermediate flow | | | | CI fall | | | | Pre-CI TLf | | | | Pre-CI TLc | | | | Pre-CI Tla | | | |
|---|---|---|---|---|---|---|---|---|---|---|---|---|---|---|---|---|---|---|---|---|---|---|---|---|
| Percentile | 80 | 60 | 40 | 20 | 80 | 60 | 40 | 20 | 80 | 60 | 40 | 20 | 80 | 60 | 40 | 20 | 80 | 60 | 40 | 20 | 80 | 60 | 40 | 20 |
| Sample | OF3B/08-20 | OF3B/08-19 | OF3B/08-10 | OF3B/08-6 | Mond152A2_08-4 | Mond15U3-8 | Mond15U3-11 | Mond15U3-2 | CIVOS 60-70-17 | OF 16A_08-10 | CIVOS 100-110-17 | CIVOS 100-110-27 | OCF 9601 F3-15 | OCF 9601 F3-12 | OCF 9550-15 | OCF 9601 F3-13 | OCF 9601 C1-14 | OCF 9601 C24-11 | OCF 9601 C24-6 | OCF 9601 C24-15 | TLa_08-2 | OCF 9601 A1-10 | OCF 9601 A1-7 | OCF 9601 A1-6 |
| Ti | 2314 | 2352 | 2304 | 2361 | 2308 | 2210 | 2334 | 2275 | 2436 | 2741 | 2351 | 2253 | 2356 | 2501 | 2532 | 2380 | 2234 | 2289 | 2361 | 2164 | 2275 | 2183 | 2205 | 2231 |
| V | 64 | 37 | 28 | 22 | 14 | 13 | 14 | 13 | 14 | 14 | 16 | 16 | 21 | 21 | 21 | 22 | 14 | 12 | 13 | 12 | 13 | 13 | 12 | 13 |
| Rb | 324 | 373 | 437 | 382 | 436 | 453 | 447 | 434 | 420 | 487 | 473 | 465 | 447 | 426 | 418 | 436 | 476 | 460 | 453 | 466 | 494 | 468 | 460 | 467 |
| Sr | 378 | 233 | 71 | 42 | 44 | 39 | 28 | 25 | 65 | 36 | 33 | 25 | 41 | 35 | 32 | 30 | 15 | 15 | 14 | 13 | 16 | 15 | 14 | 14 |
| Y | 20 | 32 | 36 | 50 | 50 | 49 | 52 | 46 | 49 | 54 | 52 | 51 | 44 | 47 | 47 | 46 | 57 | 61 | 60 | 56 | 61 | 60 | 61 | 62 |
| Zr | 173 | 335 | 405 | 598 | 610 | 582 | 616 | 560 | 660 | 660 | 650 | 615 | 527 | 580 | 569 | 548 | 746 | 762 | 751 | 704 | 761 | 748 | 768 | 780 |
| Nb | 29 | 61 | 74 | 114 | 115 | 110 | 113 | 112 | 119 | 120 | 119 | 117 | 101 | 109 | 107 | 107 | 144 | 145 | 145 | 142 | 145 | 146 | 149 | 151 |
| Ba | 573 | 251 | 73 | 34 | 15 | 19 | 15 | 17 | 32 | 33 | 22 | 19 | 16 | 9 | 9 | 8 | 10 | 6 | 6 | 6 | 9 | 6 | 6 | 6 |
| La | 44 | 72 | 85 | 121 | 119 | 115 | 119 | 113 | 115 | 128 | 125 | 121 | 106 | 117 | 114 | 111 | 136 | 142 | 141 | 132 | 144 | 142 | 146 | 147 |
| Ce | 83 | 139 | 162 | 232 | 230 | 219 | 229 | 215 | 200 | 238 | 235 | 231 | 209 | 220 | 213 | 214 | 267 | 272 | 270 | 253 | 277 | 275 | 282 | 289 |
| Pr | 9 | 14 | 16 | 23 | 23 | 22 | 23 | 22 | 22 | 25 | 24 | 23 | 21 | 23 | 21 | 21 | 26 | 28 | 27 | 25 | 27 | 27 | 28 | 29 |
| Nd | 33 | 51 | 59 | 80 | 80 | 75 | 80 | 72 | 73 | 85 | 84 | 81 | 72 | 77 | 74 | 74 | 90 | 93 | 94 | 87 | 96 | 93 | 97 | 98 |
| Sm | 6.1 | 8.5 | 10.4 | 14.4 | 13.4 | 13.2 | 13.5 | 11.8 | 13.4 | 15.2 | 14.7 | 13.8 | 13.2 | 13.2 | 12.8 | 12.5 | 15.4 | 15.7 | 15.9 | 14.0 | 16.3 | 15.9 | 17.4 | 16.9 |
| Eu | 2.0 | 1.6 | 1.6 | 1.3 | 1.4 | 1.2 | 1.3 | 1.3 | 1.1 | 1.2 | 1.3 | 1.3 | 1.7 | 1.8 | 1.7 | 1.6 | 1.4 | 1.6 | 1.5 | 1.3 | 1.4 | 1.5 | 1.5 | 1.6 |
| Gd | 4.4 | 7.3 | 7.6 | 10.0 | 10.7 | 9.9 | 9.8 | 9.9 | 10.1 | 11.1 | 10.2 | 10.5 | 9.6 | 10.1 | 9.6 | 9.5 | 12.1 | 12.0 | 11.3 | 10.5 | 11.9 | 12.7 | 12.6 | 12.4 |
| Dy | 3.7 | 5.7 | 6.6 | 8.9 | 9.0 | 8.6 | 9.3 | 8.5 | 8.5 | 10.0 | 9.7 | 9.4 | 7.9 | 8.6 | 8.7 | 8.0 | 10.0 | 10.8 | 10.8 | 10.0 | 10.7 | 10.7 | 11.0 | 11.3 |
| Er | 1.9 | 3.2 | 3.6 | 5.1 | 5.2 | 5.0 | 5.3 | 4.9 | 4.8 | 5.5 | 5.1 | 5.0 | 4.4 | 4.9 | 4.8 | 4.7 | 6.0 | 6.0 | 5.8 | 5.6 | 6.1 | 6.0 | 6.1 | 6.2 |
| Yb | 1.8 | 3.1 | 3.7 | 5.1 | 5.5 | 4.9 | 5.4 | 4.6 | 4.7 | 5.6 | 5.6 | 5.5 | 4.1 | 4.7 | 4.8 | 4.6 | 5.6 | 6.2 | 6.1 | 5.5 | 5.9 | 6.3 | 6.3 | 6.3 |
| Lu | 0.3 | 0.5 | 0.5 | 0.7 | 0.8 | 0.8 | 0.7 | 0.7 | 0.7 | 0.8 | 0.8 | 0.8 | 0.6 | 0.7 | 0.7 | 0.6 | 0.9 | 0.9 | 0.9 | 0.8 | 0.9 | 0.9 | 0.9 | 1.0 |
| Ta | 1.4 | 3.2 | 3.5 | 5.5 | 5.4 | 5.0 | 5.3 | 4.9 | 5.7 | 5.5 | 5.7 | 5.5 | 4.6 | 5.2 | 5.0 | 5.0 | 6.6 | 7.0 | 6.8 | 6.5 | 6.7 | 6.8 | 7.0 | 7.2 |
| Th | 14 | 26 | 32 | 47 | 50 | 45 | 49 | 43 | 46 | 50 | 51 | 50 | 41 | 45 | 45 | 44 | 57 | 60 | 58 | 53 | 59 | 60 | 62 | 63 |
| U | 5 | 10 | 12 | 18 | 18 | 16 | 18 | 16 | 15 | 17 | 19 | 19 | 15 | 16 | 16 | 16 | 22 | 22 | 21 | 21 | 22 | 23 | 23 | 23 |

Table(s)

| Sample | TM-7b (PP) | | | | | TM-8 (NYT) | | | | | TM-9 (Pre-NYT) | | | | | TM-15 (Pre-NYT) | | | | |
|---|---|---|---|---|---|---|---|---|---|---|---|---|---|---|---|---|---|---|---|---|
| **Shard** | **7b-4** | **7b-5** | **7b-4** | **7b-8** | **7b-15** | **8-5** | **8-7** | **8-12** | **8-9** | **8-10** | **9-1** | **9-34** | **9-4** | **9-6** | **9-7** | **15-1** | **15-2** | **15-3** | **15-4** | **15-5** |
| **EMPA (wt. % oxide)** | | | | | | | | | | | | | | | | | | | | |
| Total | 96.23 | 95.23 | 96.23 | 97.66 | 98.07 | 97.09 | 97.23 | 96.04 | 96.71 | 95.82 | 95.31 | 99.11 | 97.49 | 98.33 | 98.53 | 96.38 | 97.70 | 95.68 | 96.50 | 96.27 |
| $SiO_2$ | 57.51 | 58.15 | 57.51 | 57.35 | 57.71 | 61.81 | 56.20 | 56.90 | 56.39 | 61.63 | 62.99 | 62.58 | 62.71 | 62.85 | 62.74 | 62.88 | 62.54 | 62.26 | 62.14 | 62.19 |
| $TiO_2$ | 0.52 | 0.49 | 0.52 | 0.55 | 0.51 | 0.41 | 0.59 | 0.58 | 0.64 | 0.45 | 0.43 | 0.48 | 0.44 | 0.44 | 0.45 | 0.36 | 0.34 | 0.37 | 0.37 | 0.37 |
| $Al_2O_3$ | 19.06 | 18.92 | 19.06 | 19.08 | 19.07 | 19.13 | 18.50 | 18.52 | 18.49 | 18.46 | 18.00 | 18.06 | 18.13 | 18.22 | 18.24 | 17.85 | 17.83 | 17.84 | 18.16 | 17.84 |
| MnO | 0.13 | 0.19 | 0.13 | 0.12 | 0.11 | 0.13 | 0.11 | 0.08 | 0.19 | 0.11 | 0.19 | 0.16 | 0.18 | 0.15 | 0.15 | 0.12 | 0.10 | 0.14 | 0.14 | 0.12 |
| MgO | 1.20 | 1.13 | 1.20 | 1.31 | 1.13 | 0.29 | 2.08 | 1.57 | 1.91 | 0.43 | 0.30 | 0.27 | 0.30 | 0.27 | 0.24 | 0.45 | 0.47 | 0.56 | 0.60 | 0.61 |
| FeO | 4.50 | 4.41 | 4.50 | 4.81 | 4.48 | 2.35 | 5.87 | 5.44 | 5.79 | 2.80 | 2.40 | 2.55 | 2.49 | 2.48 | 2.52 | 3.01 | 2.95 | 3.04 | 3.25 | 3.06 |
| CaO | 3.92 | 3.83 | 3.92 | 4.07 | 3.88 | 2.37 | 5.50 | 4.89 | 5.20 | 2.22 | 1.93 | 1.83 | 1.98 | 1.88 | 1.88 | 2.15 | 2.21 | 2.25 | 2.48 | 2.41 |
| $Na_2O$ | 3.63 | 3.40 | 3.63 | 4.04 | 3.75 | 4.06 | 3.19 | 3.15 | 3.05 | 4.56 | 5.46 | 5.33 | 5.24 | 5.18 | 5.22 | 4.13 | 4.29 | 3.77 | 3.62 | 3.62 |
| $K_2O$ | 8.88 | 8.82 | 8.88 | 7.97 | 8.70 | 9.03 | 7.62 | 8.47 | 7.92 | 8.77 | 7.60 | 7.98 | 7.80 | 7.82 | 7.83 | 8.37 | 8.66 | 9.22 | 8.69 | 9.20 |
| Cl | 0.64 | 0.65 | 0.64 | 0.69 | 0.65 | 0.42 | 0.35 | 0.39 | 0.43 | 0.56 | 0.71 | 0.76 | 0.73 | 0.71 | 0.73 | 0.67 | 0.62 | 0.55 | 0.55 | 0.56 |
| **LA-ICP-MS (ppm)** | | | | | | | | | | | | | | | | | | | | |
| Ti | 2447 | 2290 | 2447 | 3510 | 3691 | 2204 | 3718 | 3483 | 3828 | 2328 | 1870 | 2557 | 2239 | 2358 | 2443 | 2190 | 2280 | 2188 | 2173 | 2077 |
| V | 97 | 91 | 97 | 125 | 143 | 51 | 152 | 145 | 173 | 54 | 31 | 37 | 34 | 35 | 35 | 37 | 38 | 44 | 44 | 43 |
| Rb | 349 | 327 | 349 | 268 | 420 | 370 | 274 | 303 | 295 | 402 | 315 | 404 | 383 | 390 | 400 | 335 | 331 | 307 | 324 | 260 |
| Sr | 736 | 680 | 736 | 722 | 1104 | 282 | 919 | 1031 | 1066 | 195 | 44 | 55 | 45 | 52 | 47 | 242 | 257 | 409 | 302 | 468 |
| Y | 23 | 21 | 23 | 20 | 30 | 30 | 24 | 23 | 26 | 30 | 34 | 40 | 35 | 37 | 36 | 29 | 28 | 23 | 24 | 21 |
| Zr | 230 | 210 | 230 | 218 | 323 | 353 | 209 | 231 | 229 | 369 | 377 | 478 | 425 | 431 | 425 | 339 | 328 | 243 | 273 | 232 |
| Nb | 39 | 38 | 39 | 39 | 56 | 58 | 33 | 37 | 37 | 61 | 66 | 78 | 74 | 73 | 73 | 51 | 49 | 37 | 47 | 32 |
| Ba | 1530 | 1399 | 1530 | 1774 | 2195 | 82 | 1599 | 2194 | 2060 | 72 | 7 | 12 | 6 | 9 | 6 | 256 | 169 | 306 | 402 | 488 |
| La | 54 | 50 | 54 | 53 | 78 | 79 | 50 | 58 | 61 | 81 | 78 | 98 | 87 | 88 | 87 | 66 | 64 | 53 | 56 | 48 |
| Ce | 115 | 101 | 115 | 104 | 158 | 150 | 98 | 114 | 122 | 155 | 152 | 192 | 177 | 180 | 174 | 125 | 123 | 100 | 107 | 91 |
| Pr | 12 | 11 | 12 | 11 | 16 | 16 | 11 | 12 | 13 | 16 | 16 | 18 | 17 | 17 | 18 | 13 | 13 | 10 | 11 | 9 |
| Nd | 44 | 38 | 44 | 42 | 59 | 57 | 40 | 46 | 50 | 57 | 55 | 68 | 64 | 65 | 61 | 49 | 48 | 43 | 42 | 35 |
| Sm | 7.9 | 6.9 | 7.9 | 7.6 | 10.4 | 9.2 | 8.4 | 8.3 | 9.6 | 9.5 | 8.5 | 10.7 | 10.7 | 10.6 | 10.5 | 8.5 | 9.5 | 7.2 | 8.9 | 5.3 |
| Eu | 1.8 | 1.5 | 1.8 | 1.8 | 2.6 | 2.1 | 2.0 | 2.2 | 2.3 | 2.1 | 1.4 | 1.9 | 1.5 | 1.7 | 1.5 | 1.8 | 1.8 | 1.7 | 1.5 | 1.7 |
| Gd | 5.8 | 5.4 | 5.8 | 5.3 | 8.1 | 7.6 | 5.5 | 6.3 | 8.1 | 7.3 | 6.9 | 8.6 | 7.9 | 7.5 | 7.0 | 6.2 | 6.2 | 5.5 | 6.7 | 4.7 |
| Dy | 4.1 | 3.4 | 4.1 | 4.1 | 5.7 | 5.5 | 4.6 | 4.6 | 5.2 | 5.6 | 5.8 | 6.9 | 6.1 | 6.7 | 6.5 | 5.3 | 5.2 | 4.3 | 4.6 | 3.9 |
| Er | 2.1 | 1.8 | 2.1 | 2.1 | 3.0 | 3.0 | 2.4 | 2.3 | 2.5 | 3.1 | 2.9 | 4.1 | 3.2 | 3.8 | 3.3 | 2.9 | 2.9 | 2.4 | 2.2 | 1.9 |
| Yb | 2.1 | 1.8 | 2.1 | 2.2 | 2.7 | 3.1 | <LOD | 2.1 | 2.2 | 3.0 | 2.6 | 4.2 | 3.7 | 3.4 | 3.5 | 2.9 | 2.8 | 2.1 | 2.4 | 2.3 |
| Lu | <LOD | <LOD | <LOD | 0.3 | <LOD | 0.5 | 0.4 | 0.3 | 0.4 | 0.4 | 0.5 | 0.5 | 0.6 | 0.5 | 0.5 | 0.4 | 0.4 | 0.3 | <LOD | 0.3 |
| Ta | 2.7 | 1.9 | 2.7 | 1.8 | 2.5 | 3.1 | 1.7 | 1.7 | 1.8 | 2.8 | 3.2 | 3.7 | 3.9 | 3.9 | 3.6 | 2.6 | 2.6 | 1.8 | 2.3 | 1.6 |
| Th | 22 | 19 | 22 | 21 | 29 | 35 | 17 | 21 | 22 | 34 | 37 | 44 | 40 | 41 | 40 | 30 | 28 | 20 | 22 | 18 |
| U | 8 | 8 | 8 | 7 | 11 | 11 | 5 | 7 | 7 | 12 | 11 | 14 | 13 | 13 | 13 | 10 | 9 | 7 | 8 | 6 |

Continues next page

| Sample | TM-18 top (CI co-ignimbrite) | | | | | TM-18 base (CI fall) | | | | |
|---|---|---|---|---|---|---|---|---|---|---|
| shard | 18t-2 | 18t-3 | 18t-6 | 18t-8 | 18t-9 | 18b-4 | 18b-19 | 18b-10 | 18b-14 | 18b-19 |
| **EMPA (Wt. % oxide)** | | | | | | | | | | |
| Total | 97.64 | 97.17 | 99.00 | 100.55 | 97.66 | 97.95 | 98.05 | 97.92 | 95.78 | 98.05 |
| $SiO_2$ | 61.52 | 61.14 | 61.54 | 61.49 | 61.73 | 61.15 | 61.67 | 61.29 | 61.55 | 61.67 |
| $TiO_2$ | 0.37 | 0.37 | 0.44 | 0.42 | 0.40 | 0.44 | 0.45 | 0.45 | 0.44 | 0.45 |
| $Al_2O_3$ | 18.58 | 18.18 | 18.66 | 18.32 | 18.21 | 18.53 | 18.41 | 18.20 | 18.30 | 18.41 |
| MnO | 0.22 | 0.13 | 0.28 | 0.20 | 0.30 | 0.24 | 0.19 | 0.20 | 0.28 | 0.19 |
| MgO | 0.30 | 0.81 | 0.33 | 0.28 | 0.32 | 0.29 | 0.31 | 0.33 | 0.35 | 0.31 |
| FeO | 3.06 | 3.39 | 2.90 | 2.98 | 2.84 | 2.96 | 2.85 | 2.86 | 2.90 | 2.85 |
| CaO | 1.65 | 2.75 | 1.63 | 1.66 | 1.68 | 1.75 | 1.63 | 1.75 | 1.72 | 1.63 |
| $Na_2O$ | 6.28 | 3.41 | 6.62 | 6.38 | 5.79 | 6.66 | 6.42 | 6.85 | 6.41 | 6.42 |
| $K_2O$ | 7.12 | 9.48 | 6.76 | 7.34 | 7.85 | 7.19 | 7.15 | 7.18 | 7.19 | 7.15 |
| Cl | 0.90 | 0.35 | 0.83 | 0.94 | 0.87 | 0.79 | 0.91 | 0.88 | 0.86 | 0.91 |
| **LA-ICP-MS (ppm)** | | | | | | | | | | |
| Ti | 2667 | 2244 | 2590 | 2648 | 2249 | 2495 | 2518 | 2478 | 2154 | 2518 |
| V | 18 | 62 | 15 | 18 | 14 | 14 | 13 | 19 | 13 | 13 |
| Rb | 452 | 289 | 459 | 448 | 437 | 439 | 430 | 493 | 419 | 430 |
| Sr | 29 | 585 | 22 | 43 | 20 | 22 | 18 | 40 | 22 | 18 |
| Y | 54 | 21 | 56 | 55 | 47 | 54 | 50 | 47 | 45 | 50 |
| Zr | 639 | 185 | 667 | 643 | 569 | 628 | 626 | 584 | 549 | 626 |
| Nb | 118 | 31 | 120 | 119 | 103 | 114 | 113 | 118 | 99 | 113 |
| Ba | 50 | 798 | 17 | 50 | 24 | 35 | 14 | 102 | 48 | 14 |
| La | 124 | 45 | 127 | 125 | 110 | 123 | 119 | 115 | 108 | 119 |
| Ce | 241 | 88 | 246 | 243 | 213 | 234 | 230 | 224 | 212 | 230 |
| Pr | 23 | 10 | 25 | 24 | 21 | 24 | 23 | 24 | 21 | 23 |
| Nd | 81 | 36 | 87 | 83 | 77 | 81 | 80 | 73 | 76 | 80 |
| Sm | 15.0 | 6.5 | 15.1 | 14.1 | 12.7 | 14.1 | 13.1 | 14.7 | 12.1 | 13.1 |
| Eu | 1.4 | 1.8 | 1.4 | 1.5 | 1.3 | 1.4 | 1.2 | <LOD | 1.2 | 1.2 |
| Gd | 10.8 | 5.2 | 10.8 | 10.6 | 10.2 | 9.5 | 10.2 | 10.5 | 8.3 | 10.2 |
| Dy | 9.1 | 3.8 | 9.3 | 9.3 | 7.7 | 9.5 | 8.8 | 8.9 | 8.1 | 8.8 |
| Er | 5.0 | 1.8 | 5.7 | 5.0 | 4.4 | 5.1 | 5.0 | 4.9 | 4.2 | 5.0 |
| Yb | 5.2 | 1.7 | 5.5 | 5.2 | 4.5 | 5.7 | 5.3 | 5.2 | 4.2 | 5.3 |
| Lu | 0.8 | 0.3 | 0.8 | 0.8 | 0.7 | 0.8 | 0.8 | 0.6 | 0.6 | 0.8 |
| Ta | 5.9 | 1.5 | 5.9 | 5.5 | 5.0 | 5.2 | 5.3 | 5.3 | 4.3 | 5.3 |
| Th | 50 | 15 | 53 | 51 | 43 | 50 | 48 | 45 | 41 | 48 |
| U | 17 | 5 | 19 | 18 | 15 | 18 | 17 | 18 | 15 | 17 |

**Table(s)**

| Sample | PP | NYT-UM | NYT-LM | | Pre-NYT VRb | Pre-NYT VRa | | Pre-NYT PRa | Pre-NYT TLo | CI upper flow | CI lower/inter mediate flow | CI fall | Pre-CI TLf | Pre-CI TLc | Pre-CI Tla |
|---|---|---|---|---|---|---|---|---|---|---|---|---|---|---|---|
| Range of compositions | variable | variable | bimodal | | narrow range | bimodal | | narrow range | narrow range | highly variable | variable | variable | narrow range | narrow range | narrow range |
| Units | all | all | LM3, LM13 | LM1 | all | A3 | A2 | all | all | all | all | all | all | all | all |
| TAS* classification | phonolite | phonolite-trachyte | phonolite-trachyte | trachyte | trachyte | phonolite-trachyte | trachyte | trachyte | trachyte | trachyte | trachyte-phonolite | trachyte-phonolite | phonolite | phonolite | phonolite |
| Diagnostic fingerprints for PP/NYT-series and CI-series | | | | | | | | | | | | | | | |
| FeO/CaO | 1.2±0.1 | 1.2±0.2 | 1.2±0.2 | | 1.2±0.1 | 1.3±0.1 | | 1.3±0.2 | 1.6±0.2 | 1.3-2.2 | 1.8±0.1 | 1.6±0.2 | 1.6±0.1 | 1.7±0.1 | 1.8±0.3 |
| Nb/Th | 1.7±0.1 | 1.7±0.2 | 1.7±0.2 | | 1.9±0.3 | 1.9±0.1 | | 1.8±0.1 | 1.6±0.1 | 2.1-2.5 | 2.4±0.2 | 2.4±0.2 | 2.5±0.2 | 2.5±0.1 | 2.4±0.1 |
| Zr/Th | 10.5±0.5 | 10.6±0.7 | 10.8±1.0 | | 11.2±1.1 | 12.1±0.7 | | 10.7±0.4 | 10.5±0.6 | 11.8-13.4 | 12.7±0.6 | 13.2±1.1 | 12.8±0.5 | 12.9±0.6 | 12.5±0.4 |
| Y/Th | 1.00±0.08 | 1.02±0.19 | 1.04±0.14 | | 1.01±0.13 | 1.11±0.11 | | 0.97±0.04 | 0.70±0.06 | 1.0-1.5 | 1.06±0.06 | 1.06±0.09 | 1.06±0.05 | 1.01±0.05 | 0.99±0.05 |
| Ta/Th | 0.08±0.01 | 0.08±0.01 | 0.08±0.01 | | 0.09±0.01 | 0.09±0.01 | | 0.09±0.01 | 0.07±0.01 | 0.10-0.13 | 0.11±0.01 | 0.11±0.01 | 0.11±0.01 | 0.11±0.01 | 0.11±0.00 |
| Cl | 2.3±0.4 | 0.42±0.13 | 0.39±0.03 | 0.56±0.06 | 0.45±0.06 | 0.42±0.05 | 0.49±0.11 | 0.47±0.07 | 0.62±0.06 | 0.24-0.62 | 0.85±0.07 | 0.63±0.06 | 0.75±0.05 | 0.83±0.06 | 0.81±0.08 |
| V | 107±14 | 91±84 | 126±18 | 57±4 | 51±8 | 121±14 | 38±5 | 53±5 | 23±4 | 15-64 | 14±2 | 16±4 | 21±3 | 12±1 | 13±1 |
| Ratios for distinguishing between series members (PP/NYT and CI) | | | | | | | | | | | | | | | |
| Nb/Ti | 0.016 ±0.003 | 0.017 ±0.01 | 0.013 ±0.002 | 0.023 ±0.000 | 0.023 ±0.002 | 0.012 ±0.001 | 0.022 ±0.004 | 0.023 ±0.002 | 0.048 ±0.006 | 0.01-0.05 | 0.048 ±0.004 | 0.047 ±0.005 | 0.044 ±0.003 | 0.063 ±0.003 | 0.066 ±0.004 |
| Y/Ti | 0.009 ±0.002 | 0.010 ±0.01 | 0.008 ±0.001 | 0.013 ±0.001 | 0.013 ±0.002 | 0.007 ±0.000 | 0.013 ±0.002 | 0.013 ±0.001 | 0.021 ±0.002 | 0.008-0.021 | 0.021 ±0.002 | 0.021 ±0.002 | 0.019 ±0.001 | 0.025 ±0.001 | 0.027 ±0.001 |
| V/Th | 4.3±0.8 | 3.6±4.3 | 4.9±1.5 | 1.7±0.4 | 1.7±0.6 | 5.7±1.0 | 1.4±0.3 | 1.7±0.3 | 0.3±0.1 | 0.3-4.7 | 0.32±0.08 | 0.32±0.11 | 0.49±0.07 | 0.21±0.02 | 0.21±0.03 |
| Ba/Sr | 1.93-2.17 | 0.3-2.2 | 1.69-1.81 | 0.33-0.68 | 0.22-0.61 | 1.65-1.78 | 0.18-0.48 | 0.40-0.68 | 0.17-0.35 | 0.4-1.5 | 0.23-1.07 | 0.18-1.15 | 0.20-0.53 | 0.40-0.75 | 0.36-0.74 |
| $Eu/Eu_N$* | 0.65-0.94 | 0.43-1.01 | 0.73-0.84 | 0.63-0.64 | 0.57-0.75 | 0.76-0.82 | 0.58-0.79 | 0.62-0.73 | 0.29–0.35 | 0.3-1.1 | 0.27-0.36 | 0.24-0.34 | 0.38-0.52 | 0.29-0.35 | 0.29-0.42 |
| Zr/Sr | 0.27-0.36 | 0.2-7.3 | 0.29-0.40 | 1.15-1.75 | 0.92-2.42 | 0.34-0.37 | 0.94-2.58 | 0.98-1.54 | 30-59 | 0-39 | 8-28 | 5-31 | 9-22 | 41-58 | 17-56 |

Table(s)

| Event | proximal age (cal ka BP) | | volume ($km^3$) and dispersal | | | distal tephra | core | location | direction | Distance (km) | thickness | age (cal ka BP) | reference |
|---|---|---|---|---|---|---|---|---|---|---|---|---|---|
| PP | 11.915-12.158 ($^{14}C$) | Smith et al., 2011 | 0.644 DRE | E | DiRienzo et al., 2011 | TM-7b L5 | LGM-B/D/E/J | Lago Grande di Monticcio | E | 120 | 47 mm | 11.571-12.789 (varve) | Wulf et al., 2004, 2008; Narcisi et al., 1996 |
| | 11.978-12.390 (Ar/Ar) | Di Vito et al., 1999 | 0.14 DRE | E | Lirer, 2001 | C-1 | KET8218 | South Adriatic | E | 310 | visible | | Paterne 1988 |
| | | | 1.78 bulk | ENE | Sulpizio, 2005 | | MD90-917 | South Adriatic | E | 330 | visible | 12.003-12.579 ($^{14}C$) | Siani et al., 2004 |
| | | | | | | | IN68-5, IN68-9 | South Adriatic | E | 440, 400 | visible | | Calanchi et al., 2008 |
| | | | | | | | Bled C | Lake Bled, Slovenia | N | 620 | crypto | | Lane et al., 2011 |
| NYT | 14.500-15.300 (Ar/Ar) | Deino et al., 2004 | >40 DRE | NE | Orsi, 1992 | TM-8 L6 | LGM-B/D/E/J | Lago Grande di Monticcio | E | 120 | 22 mm | 13.414-14.826 (varve) | Wulf et al., 2004, 2008; Narcisi et al., 1996 |
| | | | | | | C-2 | KET8218 | South Adriatic | E | 310 | visible | | Paterne 1988 |
| | | | | | | | KET8022, KET8004 | Tyrrhenian | W, SW | 200, 135 | visible | | Paterne 1988 |
| | | | | | | | PRAD218 | Central Adriatic | NE | 240 | crypto | | Bourne et al., 2010 |
| | | | | | | | CM92-43, PAL94-66, IN68-21, PAL94-8, CM92-42, CM92-41, RF93-77, PAL94-77 | Central Adriatic | NE | 200-240 | crypto | | Calanchi et al., 1998 |
| | | | | | | | MD90-917 | South Adriatic | E | 330 | visible | 13.846-14.881 ($^{14}C$) | Siani et al., 2004 |
| NYT-LM | | | >10 DRE | E | Woheltz et al., 1995 | | Bled C | Lake Bled, Slovenia | N | 620 | crypto | | Lane et al., 2011 |
| | | | | | | | LAENG1 | Längsee, Austria | N | 650 | visible | | Schmidt et al., 2002 |
| NYT-UM | | | >30 DRE | NE | Woheltz et al., 1995 | | | | | | | | |
| CI | 39.170-39.390 (Ar/Ar) | Di Vivo et al., 2001 | 105-210 DRE | NE | Pyle et al., 2006 | TM-18 L12 | LGM-B/D/E/J | Lago Grande di Monticcio | E | 120 | 257 (170 mm fall) | 34.934-38.611 (varve) | Wulf et al., 2004, 2008; Narcisi et al., 1996 |
| | | | 200 DRE | ENE to S | Rolandi et al., 2003 | | OT702-6, JO2004Y5, PR628 | Lakes Ohrid and Prespa, Macedonia | E | 340 | visible | | Sulpizio et al., 2010 ; Caron et al., 2010 ; Wagner et al., 2008 ; Vogel et al., 2010 |
| | | | 150 DRE | | Civetta et al., 1997 | | ML01 | Lesvos, Greece | E | 660 | visible | | Margari et al., 2007 |
| | | | 180–280 DRE | NE | Costa et al., 2012 | | Kostenki 14, Rudkino | Kostenki-Borschevo, Russia | ENE | 1390 | visible | | Pyle et al., 2006 |
| | | | | | | Y-5 | TR172-11,19 | Aegean | SE | 935, 970 | visible | | Hardiman 1999 ; Pyle et al., 2006 |
| | | | | | | C-10 | KET 8003,4 | Tyrrhenian | W | 135 | visible | | Paterne 1988 ; Ton-That et al., 2001 |
| CI fall | | | 15 bulk | E | Rosi et al., 1999 | | | | | | | | |
| | | | 20 bulk | E | Perrotta and Scarpati, 2003 | | | | | | | | |
| CI flow | | | 80 bulk | E | Rosi et al., 1999 | | | | | | | | |
| | | | 180 bulk | ENE to S | Rolandi et al., 2003; Pyle et al,, 2006 | | | | | | | | |

Figure(s)

Click here to download high resolution image

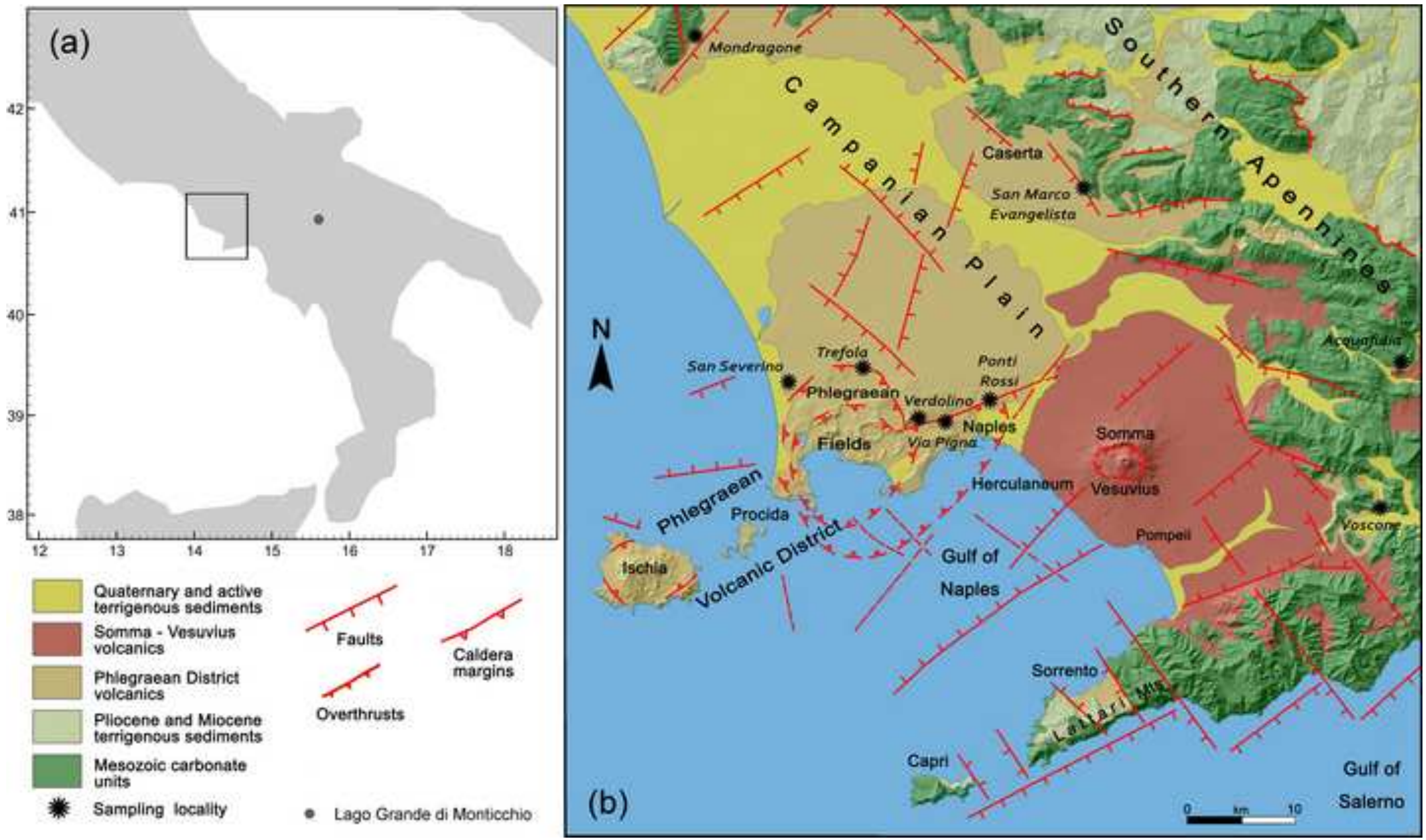

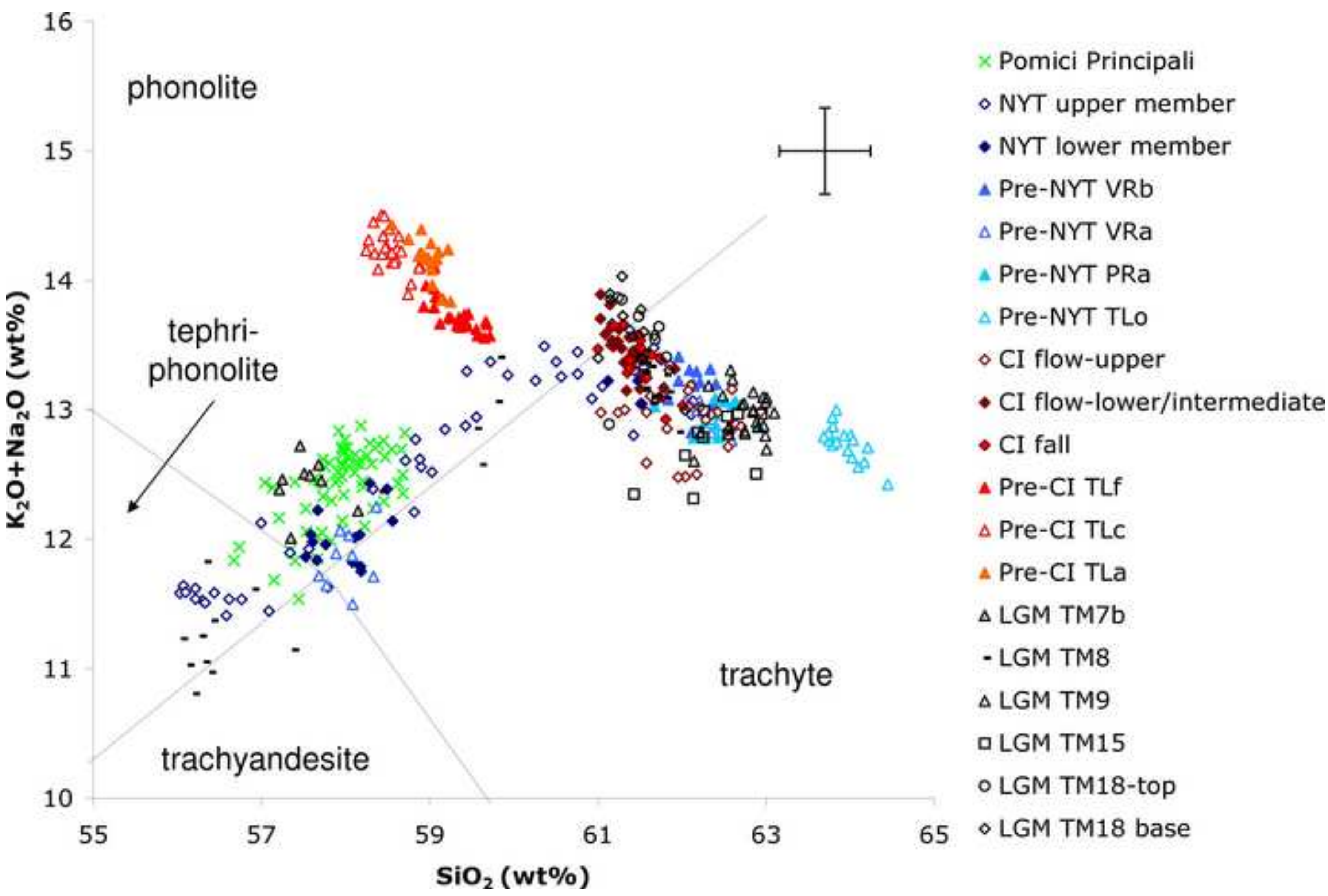
phonolite
tephri-
phonolite
trachyandesite
trachyte
$K_2O+Na_2O$ (wt%)
$SiO_2$ (wt%)
16
15
14
13
12
11
10
55
57
59
61
63
65
Pomici Principali
NYT upper member
NYT lower member
Pre-NYT VRb
Pre-NYT VRa
Pre-NYT PRa
Pre-NYT TLo
CI flow-upper
CI flow-lower/intermediate
CI fall
Pre-CI TLf
Pre-CI TLc
Pre-CI TLa
LGM TM7b
LGM TM8
LGM TM9
LGM TM15
LGM TM18-top
LGM TM18 base

Figure(s)
Click here to download high resolution image

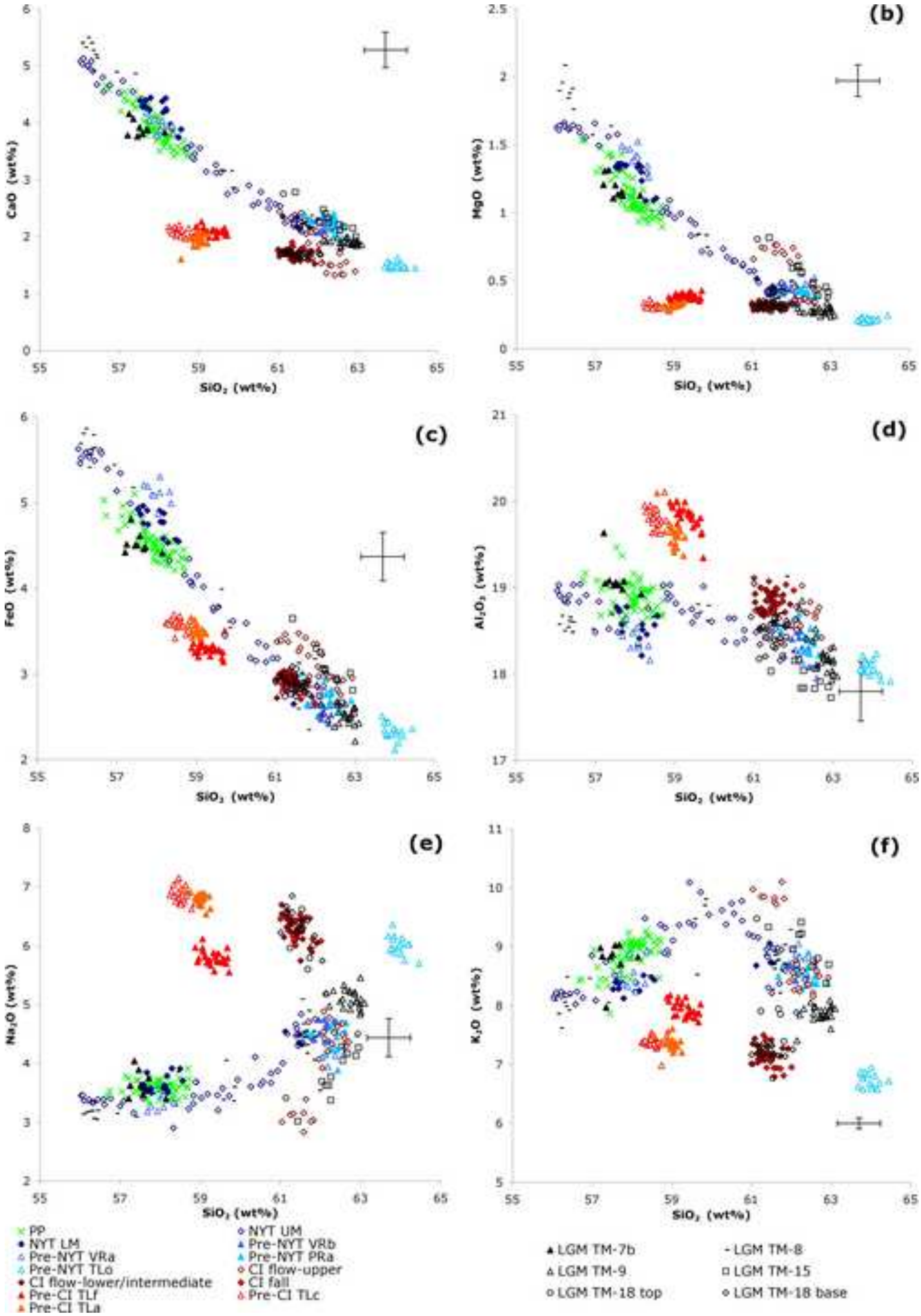

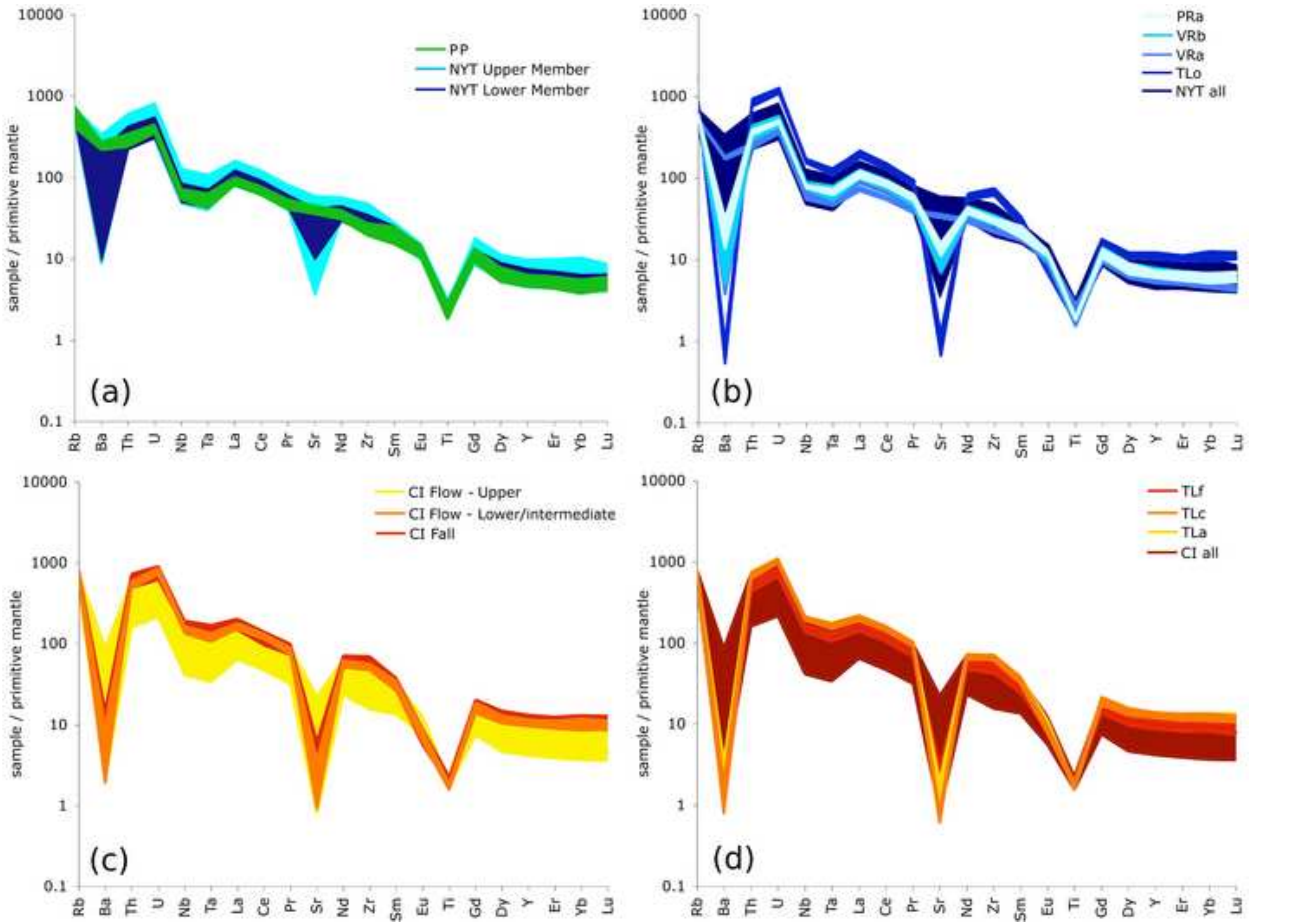
PP
NYT Upper Member
NYT Lower Member
(a)
PRa
VRb
VRa
TLo
NYT all
(b)
CI Flow - Upper
CI Flow - Lower/intermediate
CI Fall
(c)
TLf
TLc
TLa
CI all
(d)
sample / primitive mantle
10000
1000
100
10
1
0.1
Rb
Ba
Th
U
Nb
Ta
La
Ce
Pr
Sr
Nd
Zr
Sm
Eu
Ti
Gd
Dy
Y
Er
Yb
Lu

Figure(s)
Click here to download high resolution image

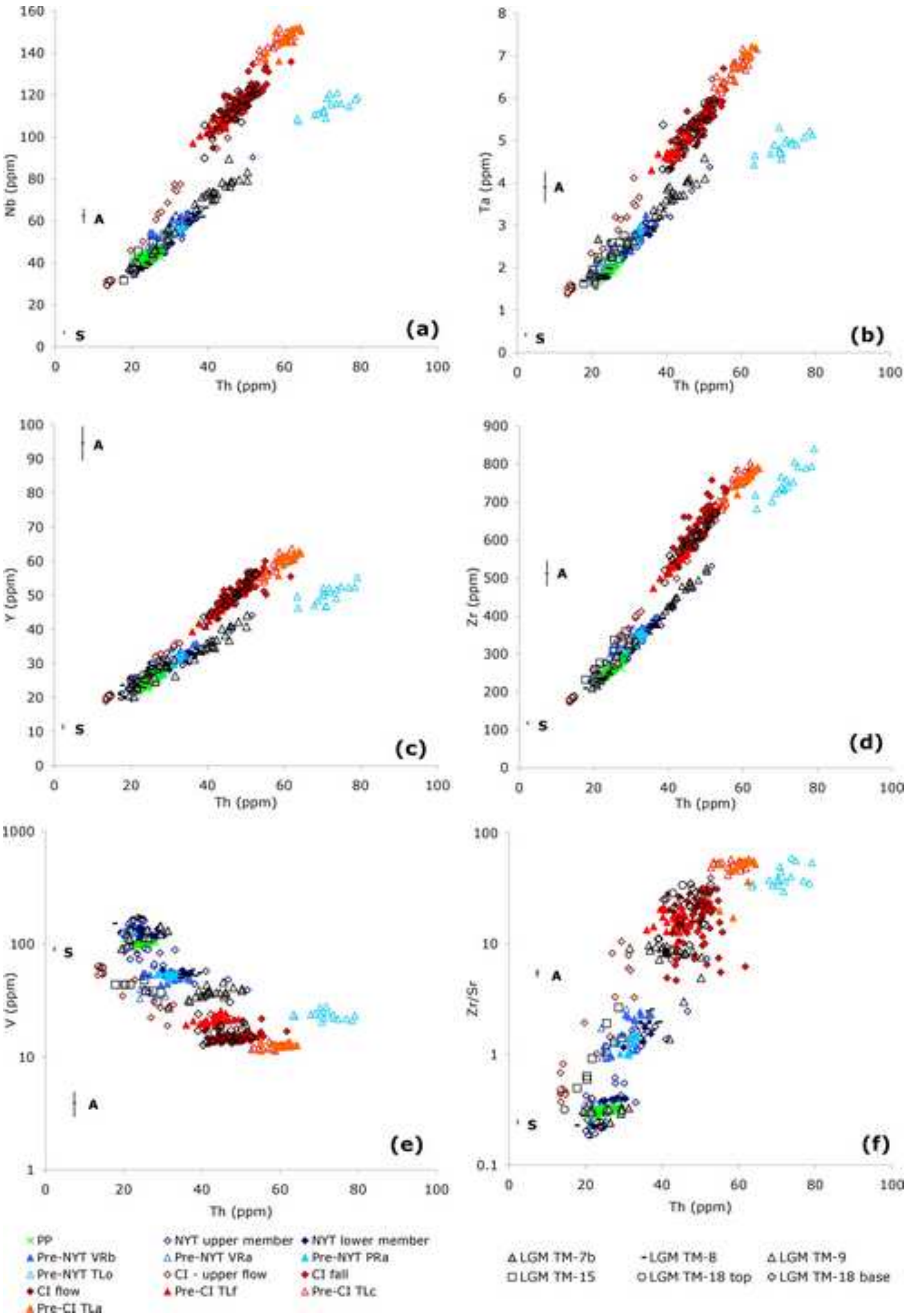

Figure(s)
Click here to download high resolution image

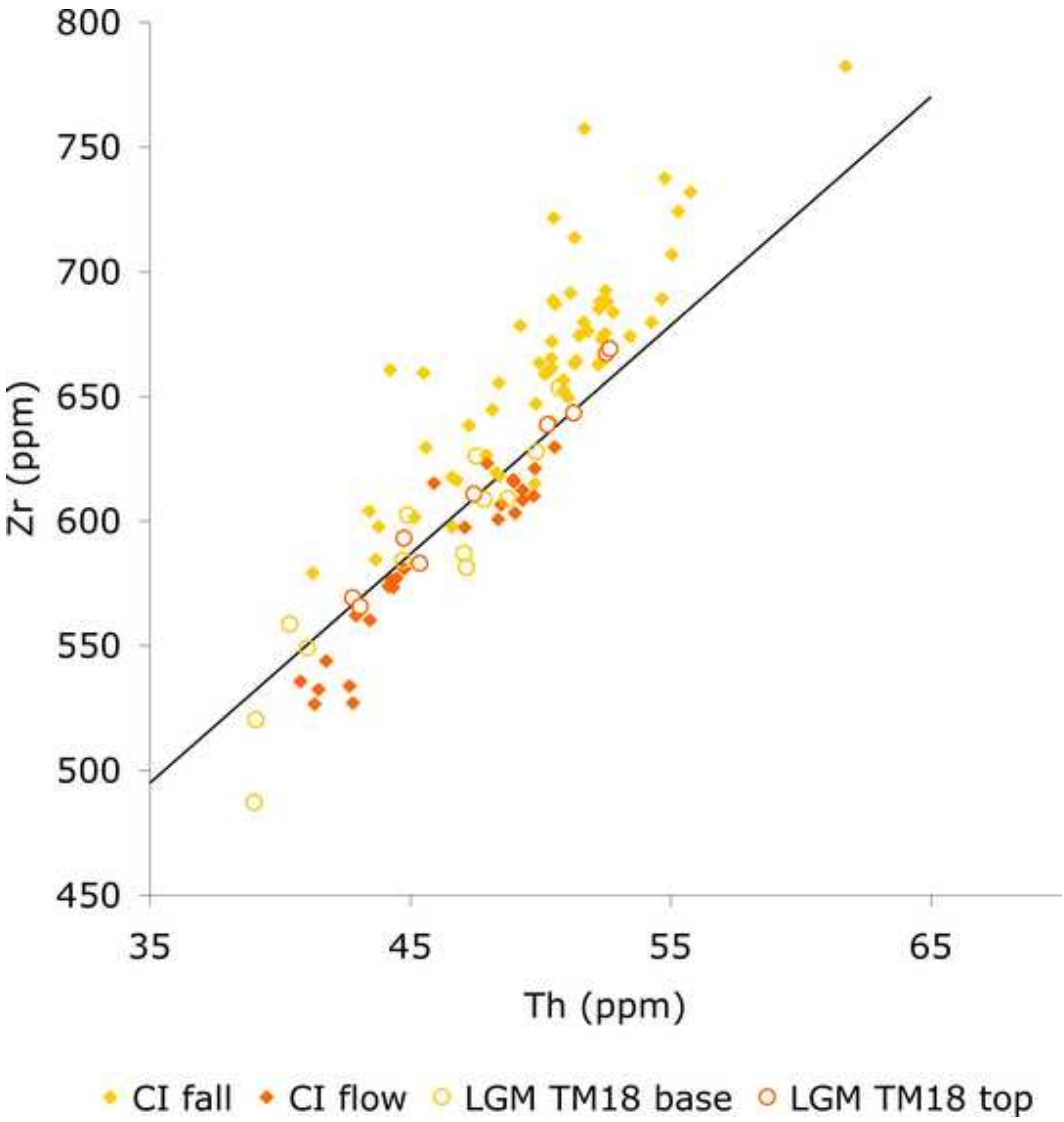

Figure(s)



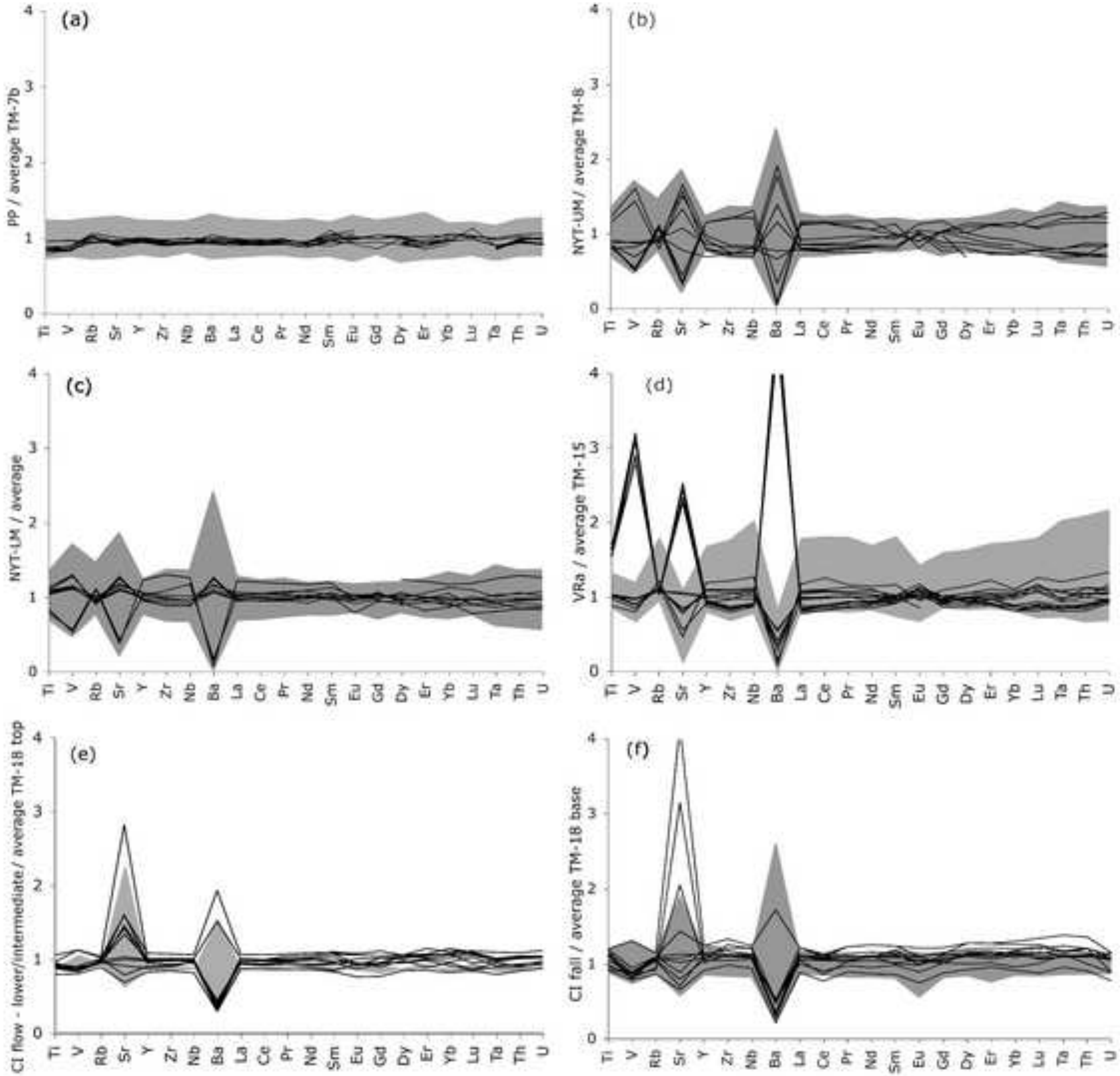
(a)
PP / average TM-7b
(b)
NYT-UM / average TM-8
(c)
NYT-LM / average
(d)
VRa / average TM-15
(e)
CI flow - lower/intermediate / average TM-18 top
(f)
CI fall / average TM-18 base
Ti V Rb Sr Y Zr Nb Ba La Ce Pr Nd Sm Eu Gd Dy Er Yb Lu Ta Th U

**Figure(s)**
**Click here to download high resolution image**

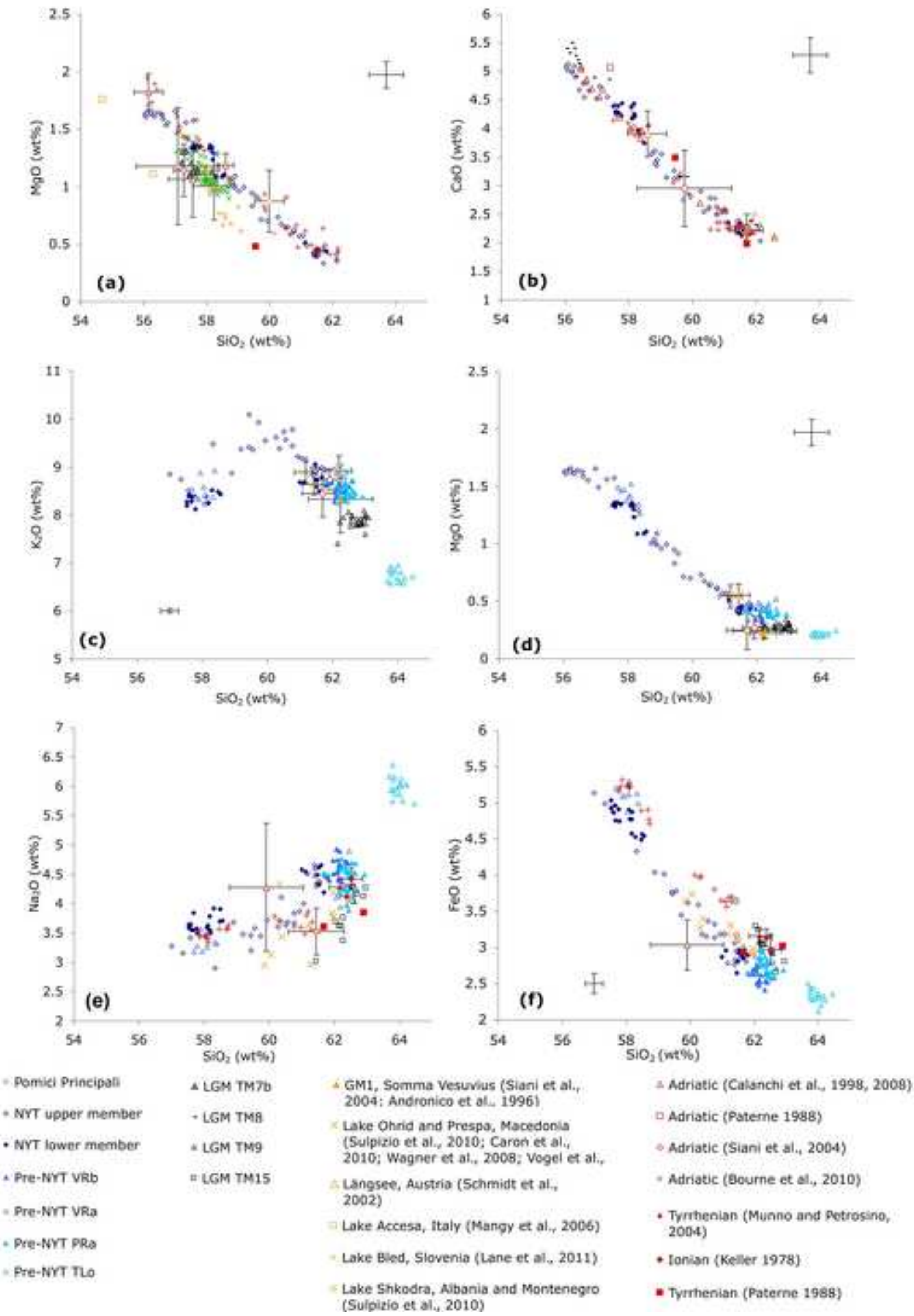

Electronic Annex
Click here to download Electronic Annex: Tomlinson_S1 (version 2).xls